DESTRUCTION OF INVARIANT CURVES IN THE RESTRICTED CIRCULAR PLANAR THREE-BODY PROBLEM BY USING COMPARISON OF ACTION

JOSEPH GALANTE and VADIM KALOSHIN

Abstract

The classical principle of least action says that orbits of mechanical systems extremize action; an important subclass are those orbits that minimize action. In this paper we utilize this principle along with Aubry-Mather theory to construct (Birkhoff) regions of instability for a certain three-body problem, given by a Hamiltonian system of 2 degrees of freedom. We believe that these methods can be applied to construct instability regions for a variety of Hamiltonian systems with 2 degrees of freedom. The Hamiltonian model we consider describes dynamics of a Sun-Jupiter-comet system, and under some simplifying assumptions, we show the existence of instabilities for the orbit of the comet. In particular, we show that a comet which starts close to an orbit in the shape of an ellipse of eccentricity $e = 0.66$ can increase in eccentricity up to $e = 0.96$. In the sequels to this paper, we extend the result to beyond $e = 1$ and show the existence of ejection orbits. Such orbits are initially well within the range of our solar system. This might give an indication of why most objects rotating around the Sun in our solar system have relatively low eccentricity.

1. Introduction

We consider the restricted circular planar three-body problem (RCP3BP) with two massive primaries, which we call the Sun and Jupiter, that perform uniform circular motion about their center of mass (see Figure 1). The system is normalized to mass 1 so that the Sun has mass $1 - \mu$ and Jupiter has mass μ. We further normalize so that Jupiter rotates with period 2π, and the distance from the Sun to Jupiter is constant and also normalized to 1. Our goal is to understand the behavior of the massless comet whose position in polar coordinates is denoted (r, ψ). It is convenient to consider the system in a rotating frame of reference which rotates with unit speed in the same
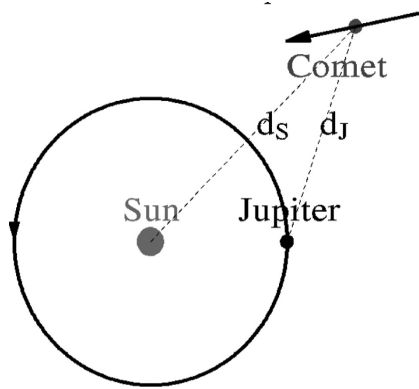
Figure 1. Sun-Jupiter-comet system

direction as Jupiter. In this system, the Sun and Jupiter are fixed points on the x-axis corresponding to $\psi = 0$. We let $(r, \varphi) = (r, \psi - t)$ denote the motion of the comet in the rotating frame of reference.

The RCP3BP has a conserved quantity known as the *Jacobi constant:*

$$J(r, \varphi, \dot{r}, \dot{\varphi}) = \frac{r^2}{2} + \frac{\mu}{d_J} + \frac{1 - \mu}{d_S} - \frac{\dot{r}^2 + r^2\dot{\varphi}^2}{2} =: U(r, \varphi) - \frac{\dot{r}^2 + r^2\dot{\varphi}^2}{2},$$

where d_J and d_S are distances to Jupiter and the Sun, respectively,

$$\begin{aligned} d_J(r, \varphi) &:= \left(r^2 - 2(1 - \mu)r\cos(\varphi) + (1 - \mu)^2\right)^{1/2} \\ d_S(r, \varphi) &:= \left(r^2 + 2\mu r\cos(\varphi) + \mu^2\right)^{1/2}. \end{aligned} \tag{1}$$

Denote by

$$\mathcal{H}(J_0) := \left\{(r, \varphi) : \ U \geq J_0\right\}$$

a set of points on the plane of motion (configuration space). Points in this set are called the *Hill regions* associated to the Jacobi constant J_0. These regions are the locations in the (r, φ)-plane (shaded regions in Figure 2) where the comet is allowed to move.

Fixing the Jacobi constant restricts dynamics to an invariant energy surface denoted

$$\mathcal{S}(J_0) := \left\{(r, \varphi, \dot{r}, \dot{\varphi}) : J(r, \varphi, \dot{r}, \dot{\varphi}) = J_0\right\}.$$

Most of these surfaces are smooth 3-dimensional manifolds. Denote by $RCP3BP(\mu, J_0)$ the RCP3BP with Sun-Jupiter mass ratio μ and dynamics restricted to the surface $\mathcal{S}(J_0)$.

It turns out that for $\mu \leq 10^{-3}$ and $J_0 \geq 1.52$ the set $\mathcal{H}(J_0)$ consists of three disjoint connected components: a region around the Sun called the *inner Hill region*, a region around Jupiter called the *lunar Hill region*, and a noncompact region called the *outer Hill region*. The boundary of these regions can be found by considering the *zero velocity* curves which are on the boundary of the Hill regions (see [AKN]). In this paper we consider only orbits contained in the outer Hill region, denoted by $\mathcal{H}^{\text{out}}(J_0)$. For convenience, denote $\mathcal{S}^{\text{out}}(J_0) = \mathcal{H}^{\text{out}}(J_0) \cap \mathcal{S}(J_0)$, and when dynamics $\mathcal{S}^{\text{out}}(J_0)$ is considered, we refer exclusively to the case when the outer Hill region is disjoint from the other two.

LEMMA 1.1

If an orbit $(r, \psi)(t)$ in $\mathcal{H}^{\text{out}}(J_0)$ makes more than one complete rotation about the origin, for example, $|\psi(T) - \psi(0)| > 3\pi$ for some $T > 0$, then $J_0^2/2 - 8\mu \leq r(t)$ for all $0 \leq t \leq T$.

This lemma is proven in Appendix B. If an orbit makes less than one rotation, then one can show that it escapes to infinity, and we are not interested in these orbits.

As the position of Jupiter is at radius $1 - \mu$, then this lemma implies, for $\mu \leq 10^{-3}$ and $J_0 \geq 1.52$, that if the comet is in an elliptic or parabolic orbit in the outer Hill region, then it remains bounded away from collisions with the Sun and Jupiter by a distance at least 8% of the Sun-Jupiter distance.

For small μ and away from collisions, the RCP3BP is nearly integrable and can be approximated with the Sun-comet two-body problem (2BP(SC)) corresponding to $\mu = 0$. Elliptic motions of a 2BP have two special points where the radial velocity $\dot{r}$ of the comet is zero. The *perihelion* is the closest point to the Sun,[†] denoted r^{perih}, and the *apohelion* is the farthest point from the Sun, denoted r^{apoh}. Define the *osculating (or instantaneous) eccentricity $e(t)$* for the RCP3BP to be the eccentricity of the comet in the unperturbed 2BP(SC) system with initial conditions taken to be those of the comet in the RCP3BP at time t.

THEOREM 1.2

Consider the RCP3BP(μ, J_0) with dynamics in $\mathcal{S}^{\text{out}}$. There exist functions $e^* = e^*(\mu, J_0)$ and $e_{\max}(\mu, J_0)$, and there exist trajectories of a comet with initial eccentricity $e^* = e^*(\mu, J_0)$ that increase to eccentricity $e_{\max}(\mu, J_0)$. For example $e^*(10^{-3}, 1.8) \leq 0.66$ and $e_{\max}(10^{-3}, 1.8) \geq 0.96$ (see Figure 3).

[†]To be pedantic, the perihelion is technically defined to be a point in the orbit when $r \leq J_0^2$ and $\dot{r} = 0$. It is *not* necessarily the closest point to the Sun. Rather it is when the comet is at the closest point to the center of mass of the system. The Sun is within μ of the center of mass. It turns out that in our solar system, the radius of the Sun is approximately 0.00089 the Sun-Jupiter distance, so we allow this slight abuse in terminology for small μ (see [NASA]).
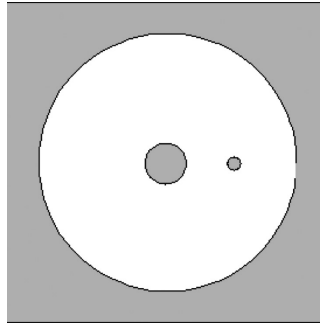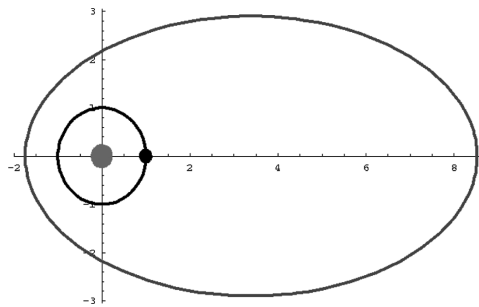
Figure 2. Hill regions

Figure 3. Ellipse of eccentricity $e = 0.66$

Suppose that $\mathcal{T}^2 \subset \mathcal{S}(J_0)$ is an invariant set of the RCP3BP(μ, J_0) that is diffeomorphic to a 2-dimensional torus. Call $\mathcal{T}^2$ *rotational* if it cannot be continuously deformed inside $\mathcal{S}(J_0)$ to a closed curve or a single point. When $\mu = 0$ (i.e., when there is no perturbation), the problem reduces to the 2BP(SC) system, and every such rotational 2-torus is defined by $\{e = e_0 \geq 0\}$. Bounded motions correspond to $e_0 \in [0, 1)$. In general, for e bounded away from 1 and μ sufficiently small, many of these rotational 2-tori survive due to KAM (see [SM]). Celletti and Chierchia [CC] gave a computer-assisted proof using $\mu \approx 10^{-3}$ and $J_0 \approx 1.76$ in the inner Hill region to show that near $e = 0.3$ there is a rotational 2-torus $\mathcal{T}^2$ separating $\mathcal{S}(J_0)$ into a compact *Below* $\mathcal{T}^2$ component and a noncompact "Above $\mathcal{T}^2$" component. Their proof may be adapted to the outer Hill region (see [CC1]). We present our method for the specific value of $J_0 = 1.8$; however, our method works for any $\mu \leq 10^{-3}$ and $J_0 \geq 1.52.$*

---

*Values $\sqrt{2} \leq J_0 \leq 1.52$ require substantial additional work as the lunar Hill region and outer Hill region are no longer disjoint. For J_0 near or less than $\sqrt{2}$, collisions with Jupiter are hard to exclude.
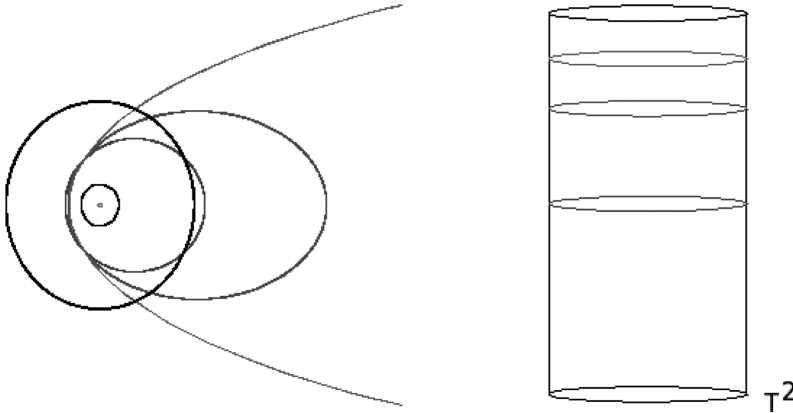
Figure 4. Various eccentricity orbits of the 2BP in the plane and on the cylinder $\mathbb{T}^2 \times I$

Define a *region of instability* (RI) for the RCP3BP(μ, J_0) as an open set in $\mathcal{S}(J_0)$ which has no rotational 2-dimensional tori inside.[†] If there is a rotational 2-torus, then it separates $\mathcal{S}(J_0)$ into an *above* and a *below* (see Section 7 for precise definitions). This provides a topological obstruction to instability. As a matter of fact, we prove the following.

THEOREM 1.3
In the setting of Theorem 1.2, the RCP3BP(μ, J_0) has a region of instability which contains the region $\{e^*(\mu, J_0) \leq e \leq e_{\max}(\mu, J_0)\}$.

This paper is the first in the sequence of three papers on instabilities for the RCP3BP. In the sequels [GK1] and [GK2] we extend this theorem and prove that the RI contains the region $\{e^* \leq e\}$.

The primary tools for this result are Aubry-Mather theory and rigorous numerical integration. It is not trivial to apply Aubry-Mather theory to the RCP3BP since the typical usage requires the RI to be an invariant domain, and we do not have such invariance in our case. We stress that trajectories are *not* constructed by means of numerical integration. After a mathematical framework is developed, we derive a list of inequalities. To have an explicit value of e^*, we use a computer to verify the range of validity of the inequalities, which are of two types: *analytic* and *dynamic*. Analytic inequalities do *not* make use of integration of the equations of motion. Dynamical inequalities *do involve integration* but only over short periods of time. We

---

[†]Birkhoff considered *invariant* regions of instability known as *Birkhoff regions of instability*. We study motions in noninvariant RIs, and special care is taken to handle issues of noninvariance.

use software which can handle both types of inequalities in a mathematically rigorous way (see Appendix A).

In the sequel [GK1], relying on Mather's variational method (see [M1], [M2], [X1], [BK]) we show that in an RI there is a full set of Chazy instabilities (see [AKN], also see [X2]). We would like to point out that existence of ejection orbits and Chazy instabilities for RCP3BP was established by Llibre and Simo [LS]. We estimate their $e^*(0.001, 1.8) \approx 0.995$; however, their motions belong to a horseshoe, while ours have a fairly different nature. Our orbits are *local action minimizers and shadow closely a collection of Aubry-Mather sets.* The idea of constructing Chazy instabilities originated in the famous paper by Sitnikov [Si] (see also [Mo3] for conceptual and transparent exposition of Sitnikov's work). Alekseyev [Al] constructed oscillatory motions for the full spatial three-body problem (3BP).

2. Roadmap to the results

Recall that motions of the comet in rotating polar coordinates (r, φ) can be viewed as the solutions to Hamilton's equations with a Hamiltonian of the form

$$H_{\text{Polar}} = H_{2BP(SC)} + \Delta H(r, \varphi) := \frac{P_r^2}{2} + \frac{P_\varphi^2}{2r^2} - P_\varphi - \frac{1}{r} + \Delta H(r, \varphi; \mu), \quad (2)$$

where P_r and P_φ are the momenta variables conjugate to r and φ, respectively (see, e.g., [AKN]), and ΔH is the μ-small perturbation of the associated 2BP(SC). This system arises by initially considering the planar 3BP, where the comet has mass m, and letting $m \to 0$. With the notation in (1), ΔH can be written

$$\Delta H := \frac{1}{r} - \frac{\mu}{d_J} - \frac{1 - \mu}{d_S} = \frac{\mu(\mu - 1)(1 + 3\cos(2\varphi))}{4r^3} + O\left(\frac{\mu}{r^4}\right).$$

The proof starts with expressing equations of motion of RCP3BP in so-called *Delaunay variables* (formally defined in Section 5). These are action angle variables of the $2BP(SC)$ or, equivalently, of $RCP3BP$ with $\mu = 0$, and have two angular variables ℓ and g in $\mathbb{T}$ and two action variables $0 \leq G \leq L$. There is a canonical transformation

$$\mathcal{D} : (\ell, L, g, G) \to (r, \varphi, P_r, P_\varphi)$$

which converts Delaunay coordinates into symplectic polar coordinates. The image consists of all bounded motions of the $2BP(SC)$. The map $\mathcal{D}$ is described in Section 5.

It turns out that there is a good 2-dimensional Poincaré section $\Gamma \subset \mathcal{S}(J_0) = \{H = -J_0\}$ of the dynamics of $RCP3BP(\mu, J_0)$ in the outer Hill region. In other words, a Poincaré map $\mathcal{F}_\mu : U \to \Gamma$ is well defined on an open set $U \subset \Gamma$ homeomorphic to an annulus (see Section 6, (10)). For $\mu = 0$ there are natural coordinates on

$\Gamma \simeq \mathbb{T} \times \mathbb{R}_+ \ni (\ell, L)$ with $\ell \in \mathbb{T}$ and $L \geq 0$. It turns out that for $\mu = 0$ and $J_0 > 1.52$, quantities

$$L = L(e, J_0) \qquad \text{and} \qquad e = e(L, J_0)$$

are monotone implicit functions of each other. On the energy surface $\mathcal{S}(J_0)$ they satisfy the implicit relation $J_0 = -1/(2L^2) - L\sqrt{1 - e^2}$. Moreover, $L \to \infty$ as $e \to 1$, and vice versa on $\mathcal{S}^{\text{out}}(J_0)$. Below we use either e or L-parameterization of the vertical (i.e., action) coordinate. When $\mu = 0$, the Poincaré map $\mathcal{F}_\mu$ has the form (cf. Figure 4)

$$\mathcal{F}_0 : (\ell, L) \to (\ell + 2\pi L^{-3}, L).$$

This map is clearly a twist map (see [MF], [B], [Mo1] for discussion of twist maps). For small μ, the corresponding Poincaré map $\mathcal{F}_\mu$ is a small perturbation of $\mathcal{F}_0$ *only for e separated away from* 1.

To prove all the results stated above it is sufficient to perform a detailed analysis of $\mathcal{F}_\mu$. Analysis of $\mathcal{F}_\mu$ naturally divides into the following stages.

Stage 1. Determine a *twist region*, denoted $\text{Tw}^{\text{Del}} = \{e_{\text{twist}}^- \leq e \leq e_{\text{twist}}^+\}$, where $\mathcal{F}_\mu$ is a twist map.

This is done by derivation of a sufficient condition to check that an infinitesimal twist holds locally uniformly. This condition says that a function of certain first and second partial derivatives of H has to be strictly negative. See Section 6 for details. The values e_{twist}^- and e_{twist}^+ are computed by numerical extremization of value of this function. It is important to notice that Tw^{Del} is *not invariant*, but is, however, compact. Even though $\mathcal{F}_\mu$ twists in Tw^{Del}, a priori there might be no invariant sets in Tw^{Del} at all.

Stage 2. Show that for each $n \geq N_0$ and each rotation number $\omega \in [1/(n+1), 1/n] \subset \mathbb{R}$ the corresponding Aubry-Mather set Σ_ω of $\mathcal{F}_\mu$ has small vertical L-deviations on the cylinder; that is, $\Sigma_\omega \subset \{(\ell, L) : L_n^- < L < L_n^+\}$.

This stage is done in [GK2] by using the ordering condition from Aubry-Mather theory. This implies that in a region slightly smaller than Tw^{Del} there are Aubry-Mather sets.

Stage 3. Rule out invariant curves to show the existence of an RI $\{e^* \leq e \leq e_{\max}\} \subset \text{Tw}^{\text{Del}}$.

This is done in the present paper. The idea is the following. Suppose that Σ_ω is an invariant curve (an example of an Aubry-Mather set) for the exact area-preserving twist (EAPT) $\mathcal{F}_\mu$, and denote by $\widetilde{\Sigma}_\omega$ a lift of Σ_ω to $\mathcal{S}(J_0)$. We prove that $\mathcal{D}^{-1}(\widetilde{\Sigma}_\omega)$ consists of action minimizers of the RCP3BP Lagrangian in polar coordinates. For ω relatively small, we show that action minimizers *cannot* visit a certain ℓ-strip on the cylinder $\mathbb{T}^2 \ni (\ell, L)$. This implies that there are no invariant curves for small
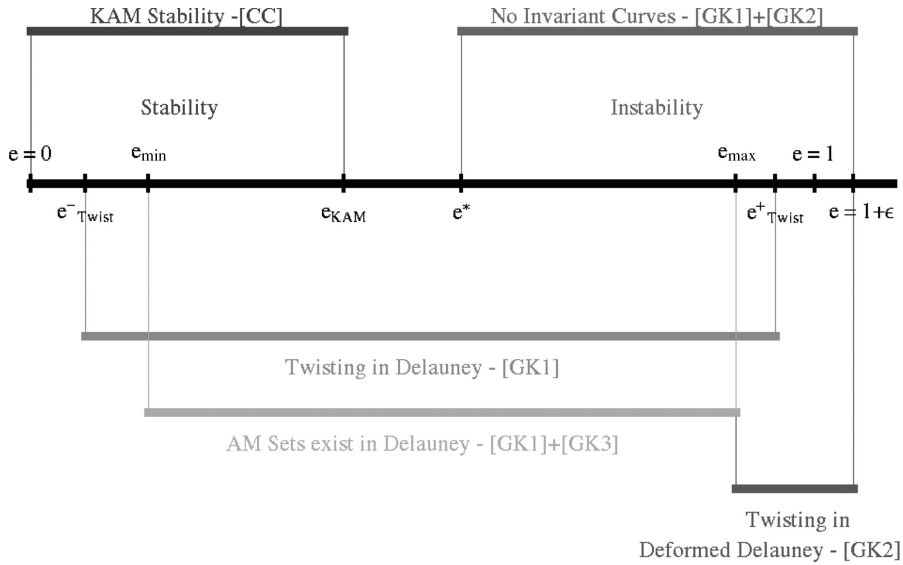
Figure 5. Roadmap of results

ω or, equivalently, for highly eccentric motions. In Section 3 we outline a heuristic method for destroying invariant curves in polar coordinates; then in Section 4 and the appendices the results are made rigorous.

Combining steps 1, 2, and 3 with Mather's variational techniques, we obtain a proof of Theorem 1.2. It might not be surprising that the twist region Tw$^{\text{Del}}$ is compact. Action-angle (Delaunay) variables are designed to describe the compact part of the dynamics, and as motions approach unbounded (parabolic) motions, usage of these coordinates becomes less and less reliable. For example, they are not defined for Aubry-Mather sets $\widetilde{\Sigma}_\omega$ with very small rotation numbers ω (see [GK1]). Thus, to prove existence of ejection/capture orbits we need to prove the existence of a semiinfinite RI in the L-direction for the map $\mathcal{F}_\mu$. This leads to analysis of the noncompact part above Tw$^{\text{Del}}$, denoted Tw$^\infty$.

Stage 4. Construct symplectic deformation of Delaunay variables so that $\mathcal{F}_\mu$ is a twist map for nearly parabolic motions.

This is done through analysis of the dynamics of the RCP3BP in symplectic polar coordinates, where all bounded motions are well defined. It turns out that arguments of Stage 3 apply to Aubry-Mather sets in Tw$^\infty$ or near the top boundary of Tw$^{\text{Del}}$ and exclude the possibility of invariant curves of any small rotation number. This shows that the RI which contains $\{e^* \leq e \leq 1 + \epsilon\}$ is semiinfinite in the L-direction. Construction of the deformed coordinate system is the primary focus of [GK1]. ([GK1] refers to the present work). The plan of the paper is the following.

(1)   In Section 3 a heuristic method for destruction of rotational tori is presented.
(2)   In Section 4 the heuristics of Section 3 are formalized via interval arithmetic, and the bounds needed to be checked via computer are laid out.
(3)   In Section 5 Delaunay variables are defined, and in Section 6 they are used to formulate the twist condition for the map $\mathcal{F}_\mu$.
(4)   The applicability of Aubry-Mather theory to the RCP3BP is found in Section 7.
(5)   The remainder of the paper is composed of lengthy technical appendices.

3. The action comparison method

"Nature is thrifty in all its actions."

Maupertuis

In this section we outline a method for destroying invariant curves based on the method of comparing actions. We illustrate the core of this method by making several simplifying assumptions which are removed in later sections.

3.1. Action minimization

The motions of the comet at position $q = (r, \varphi)$ and velocity v also satisfy the Euler-Lagrange equations with Lagrangian

$$L(r, \varphi, \dot{r}, \dot{\varphi}) = \frac{\langle v, v \rangle}{2} + \frac{1}{r} - \Delta H := \frac{\dot{r}^2}{2} + \frac{r^2(\dot{\varphi} + 1)^2}{2} + \frac{1}{r} - \Delta H(r, \varphi; \mu) \quad (3)$$

and locally minimize action.

Notice that L maps $\mathbb{R}^2 \times \mathbb{R}^2 \to \mathbb{R}$ and is a real analytic positive definite Lagrangian away from Jupiter and the Sun, for example, in $\mathcal{H}^{\mathrm{out}}(J_0)$. Let $(q_0, t_0), (q_1, t_1) \in \mathbb{R}^2 \times \mathbb{R}$. *Action* along an absolutely continuous curve $\gamma : [t_0, t_1] \to \mathbb{R}^2$ is defined to be

$$A(\gamma) = \int_{t_0}^{t_1} L\big(\gamma(t), \dot{\gamma}(t)\big)\, dt.$$

We say that a curve $\gamma : [t_0, t_1] \to \mathbb{R}^2$ is *action minimizing* if

$$A(\gamma) = \min_{\gamma:[t_0,t_1]\to\mathbb{R}^2:\gamma(t_0)=q_0,\gamma(t_1)=q_1} A(\gamma),$$

where the minimum is taken over all absolutely continuous curves connecting q_0 to q_1. We also say that a curve $\gamma : \mathbb{R} \to \mathbb{R}^2$ is *globally action minimizing* if it is action minimizing on every time interval $[t_0, t_1]$.
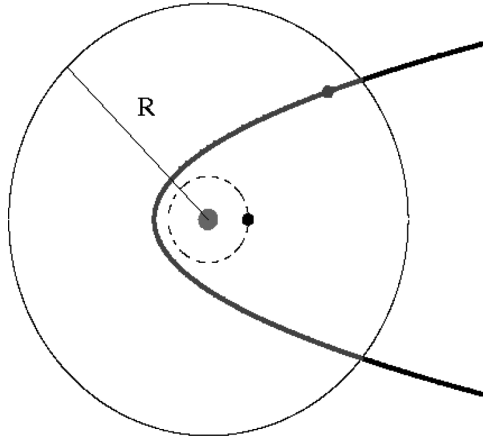
Figure 6. An R-solar passage

LEMMA 3.1

If $\mathcal{T}^2$ is a rotational 2-torus of RCP3BP, then every trajectory inside of $\mathcal{T}^2$ is globally action minimizing.

This result is proved in Section 7. However, let us consider the utility of the result now. Our goal is to show that certain high-eccentricity trajectories are *not* globally action minimizing. If this is so, then they are not contained in rotational 2-tori, and analysis of the location of these trajectories eliminates possible rotational 2-tori. (Recall that 2-tori are obstructions to diffusion.) The main idea is that passing by Jupiter is cheaper at some times than at others. We exploit this difference and outline the method for producing instabilities by using some simplifying assumptions; then in a later section we develop the formalism to make the method rigorous.

3.2. Solar passages and perihelion angles

Consider a trajectory $(r(t), \varphi(t)) \in \mathcal{S}(J_0) \cap \mathcal{H}^{\text{out}}(J_0)$ such that

(1) $r(t_1) = R$ for some time t_1;
(2)   the trajectory passes through a perihelion $r^{\text{perih}} = r(t^{\text{perih}}) < J_0^2$ at some time $t^{\text{perih}} > t_1$. Recall $P_r = \dot{r} = 0$ at the perihelion: physically it is the closest point to Sun;
(3) $r(t_2) = R$ for some time $t_2 > t^{\text{perih}}$.

   Call such a segment of trajectory $(r(t), \varphi(t))_{t \in [t_1, t_2]}$ an *R-solar passage* (see Figure 6). The *perihelion angle*, denoted φ^{perih}, is the angle the comet makes relative to the position of Jupiter when the comet is at the perihelion. Let $SP(J_0, R)$ be the set of all R-solar passages. The following lemma guarantees existence of solar passages.

LEMMA 3.2
Consider RCP3BP(μ, J_0) with $\mu \leq 10^{-3}$ and $J_0 \geq 1.52$. Suppose that $\gamma(t) = (r(t), \varphi(t)) \in \mathcal{S}^{\mathrm{out}}(J_0)$ is a trajectory such that for some sufficiently long interval of time it holds that $e(t) \geq e_0$ for some $e_0 \in (0, 1)$. Then there exists an $R_{\max}(e_0)$ such that $\gamma(t)$ has R-solar passages for all $r^{\mathrm{perih}} < R \leq R_{\max}$. Furthermore, $J_0^2/2 - 8\mu \leq r^{\mathrm{perih}} \leq J_0^2$.

We present a heuristic proof of this lemma for $J_0 = 1.8$. Recall that for the 2BP(SC), $\mu = 0$ and $\dot{e}(t) \equiv 0$. For $e \geq 0.45$ on $\mathcal{H}^{\mathrm{out}}(1.8)$, trajectories are ellipses with apohelion distance to the origin $r^{\mathrm{apoh}} \geq 5$. This indicates that there are times $t_1 < t_2$ such that $r(t_1) = r(t_2) = R \leq r^{\mathrm{apoh}}(e)$, and hence for some $t^* \in [t_1, t_2]$ we have $\dot{r}(t) < 0$ (resp., > 0) for each $t \in (t_1, t^*)$ (resp., (t^*, t_2)). This implies that $r(t^*)$ is a minimum of $r(t)$ on the interval $[t_1, t_2]$. Simple analysis of ΔH shows that $|\Delta H| \leq 2.7\mu/r^3$ for $r \geq 1.59$. This implies that $\dot{e}(t) \simeq O(\mu/r^3)$, which is small since $\mu = 10^{-3}$, so the shape of the orbit is almost unchanged and hence the minimum, that is, the perihelion, still exists under perturbation. Furthermore, since $e_0 \approx e(t)$ holds for a sufficiently long time, there exists an $R_{\max} \simeq r^{\mathrm{apoh}}(e_0)$ such that there are R-solar passages for all $r^{\mathrm{apoh}} < R \leq R_{\max}$. The lower bound on the radius follows from properties of $\mathcal{H}^{\mathrm{out}}(1.8)$ and is approached with nearly parabolic motions, while the upper bound follows from considering nearly circular motions of the comet.

This argument is made rigorous in Section 4 when we exhaustively construct a large class of 5-solar passages with computer assistance and estimate changes in $e(t)$.

3.3. Bad perihelion angles
We now prove that certain R-solar passages are not action minimizing. It turns out that this depends heavily on the perihelion angle during the passage.

THEOREM 3.3 (*Bad angles theorem*)
Consider RCP3BP(μ, J_0), and restrict dynamics to $\mathcal{S}^{\mathrm{out}}(J_0)$. There is a function $e^*(\mu, J_0)$ such that for all initial eccentricities $e_0 > e^*(\mu, J_0)$, there exists an interval $[\varphi_-, \varphi_+]$ with $\varphi_\pm = \varphi_\pm(\mu, J_0, e_0)$ such that if $(r(t), \varphi(t))_{t \in [t_1, t_2]}$ is an R-solar passage and perihelion angle $\varphi^{\mathrm{perih}} \in [\varphi_-, \varphi_+]$, then $(r(t), \varphi(t))_{t \in [t_1, t_2]}$ is not action minimizing.

A heuristic proof of the bad angles theorem is presented later in this section, and a rigorous proof is presented in Section 4. By combining Lemmas 3.2 and 3.1 and Theorem 3.3 we now show there is an $e^*(\mu, J_0)$ such that there are no rotational 2-tori crossing the region $\{e \geq e^*(\mu, J_0)\}$.
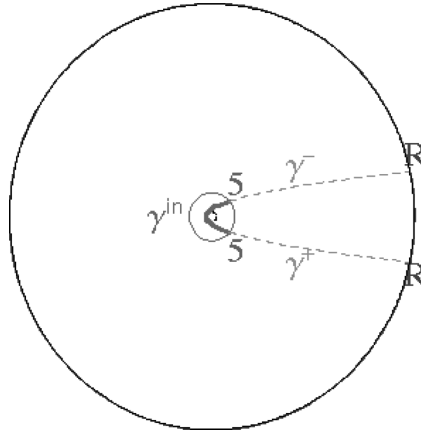
Figure 7. Decomposition of γ into smaller arcs

Proof of Theorem 1.2
The proof is by contradiction. Suppose that there is a rotational 2-torus $\mathcal{T}^2$ of RCP3BP(μ, J_0). Consider the intersection of $\mathcal{T}^2$ with perihelion/apohelion surface $\{\dot{r} = 0\}$. In polar coordinates $\dot{\varphi} < 0$, so trajectories intersect $\{\dot{r} = 0\}$ transversally, and thus $\{\dot{r} = 0\} \cap \mathcal{T}^2$ is diffeomorphic to a compact 1-dimensional manifold, that is, the circle. This implies that for every perihelion angle $\varphi^{\text{perih}} = \varphi(t^{\text{perih}})$ there is a trajectory $(r(t), \varphi(t))$ inside $\mathcal{T}^2$ with this perihelion angle. By Lemma 3.2, there is an R-solar passage $(r(t), \varphi(t))_{t \in [t_1, t_2]}$ with $t^{\text{perih}} \in [t_1, t_2]$ for this trajectory. By Theorem 3.3, this R-solar passage is *not* action minimizing, which contradicts Lemma 3.1. Thus there are no rotational 2-tori for RCP3BP(μ, J_0) crossing $\{e \geq e^*(\mu, J_0)\}$.   □

3.4. Action decomposition
In this section we stick to $\mu = 10^{-3}$ and $J_0 = 1.8$ for concreteness. Suppose that $\gamma \in SP(1.8, R)$ is an R-solar passage. We define an (R_1, R_2) *segment* as a piece of the trajectory of the RCP3BP, where the radius is monotonically increasing or decreasing from R_1 to R_2. We decompose γ into (see Figure 7):
- γ^- – an $(R, 5)$-*segment*,
- γ^{in} – a 5-solar passage,
- γ^+ – a $(5, R)$-*segment*.

Remark. For $r \geq 5$ and $\mu = 10^{-3}$, one can show that $|\Delta H| \leq 10^{-5}$. Call the region $\{r \geq 5\}$ the *outside region* since the comet is practically outside the range of influence of Jupiter. Call the region $\{r \leq 5\}$ the *kick region* because the comet's orbital parameters are perturbed (or kicked) more in this region.
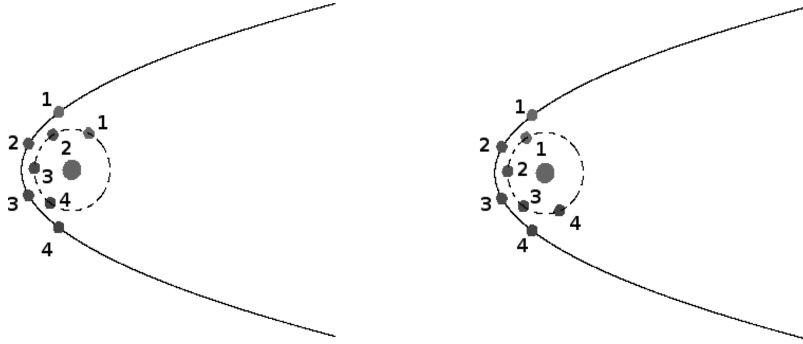
Figure 8. Potential capture (left) and escape (right) motion of the system
at times $t_1 < t_2 < t_3 < t_4$

We denote the action on each of the segments A_{out}^-, A_{in}, and A_{out}^+, respectively,

$$A(\gamma) = A_{\text{out}}^- + A_{\text{in}} + A_{\text{out}}^+.$$

3.5. Action comparison in the kick region

It turns out that A_{in} has fairly sensitive dependence on the perihelion angle. The difference in actions can be explained physically by considering two scenarios. One possibility is that the comet is pulled along behind Jupiter and gains velocity. This is a so-called *gravity assist*, and when the comet leaves the perihelion, it is flung further out than before. This case turns out to be action minimizing since the comet is getting a free ride from Jupiter. The other possibility is exactly the reverse. The comet is slowed down by Jupiter and is pulled more inward, as Jupiter attempts to capture it. Note that Jupiter can never actually capture the comet as a moon since the lunar Hill region around Jupiter is separated from the outer region by our choice of Jacobi constant.

According to standard formulas (see [AKN]), it turns out that the eccentricity $e = \sqrt{1 - 2P_\varphi^2(J_0 - P_\varphi)}$, where $J_0 = -H$, is the energy of the associated Hamiltonian. Thus one can also parameterize the 3-dimensional energy surface $\mathcal{S}(J_0)$ with coordinates (r, φ, P_φ). Denote by $SP(J_0, R, P_\varphi)$ the set of all R-solar passages belonging to $\mathcal{S}(J_0)$ that have initial angular momentum P_φ. Define $\varphi_{\max}^{\text{perih}}$ and $\varphi_{\min}^{\text{perih}}$ as the angles such that

$$A_{\text{in}}(P_\varphi, \varphi_{\max}^{\text{perih}}) := \max_{\gamma \in SP(J_0, R, P_\varphi)} A(\gamma^{\text{in}}), \qquad A_{\text{in}}(P_\varphi, \varphi_{\min}^{\text{perih}}) := \min_{\gamma \in SP(J_0, R, P_\varphi)} A(\gamma^{\text{in}}).$$

$$(4)$$

Remark. It turns out that $\varphi_{\min}^{\text{perih}}$ and $\varphi_{\min}^{\text{perih}}$ depend slightly on P_φ. Ignore this for now to keep the argument simple.
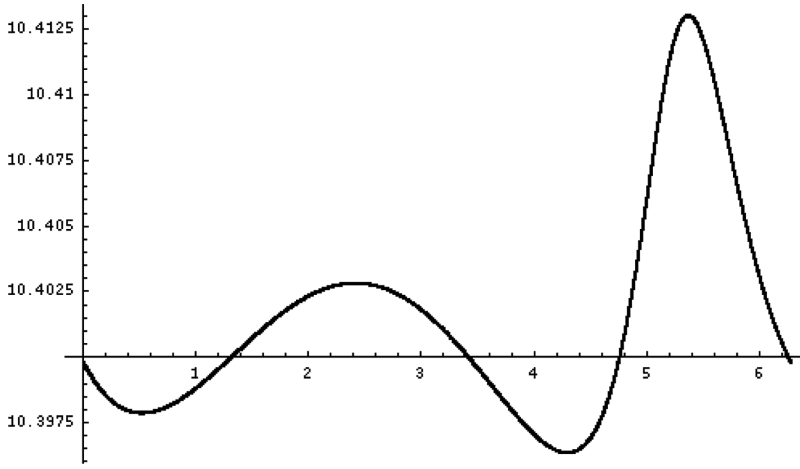
Figure 9. Action difference for nearly parabolic motions

Let us compute the differences in action and angle:

$$\Delta A_{\text{in}}^{\min} := \min_{P_\varphi} \left(A_{\text{in}}(P_\varphi, \varphi_{\max}^{\text{perih}}) - A_{\text{in}}(P_\varphi, \varphi_{\min}^{\text{perih}}) \right), \qquad \Delta\varphi := \varphi_{\max}^{\text{perih}} - \varphi_{\min}^{\text{perih}}. \tag{5}$$

To get a feel for these quantities, let us consider $R = 26$-solar passages corresponding to nearly parabolic motions ($P_\varphi \approx J_0$). A computer can then compute $\Delta A_{\text{in}}^{\min} \approx 0.0163237$ and $\Delta\varphi \approx 1.076$. A detailed algorithm for rigorously computing these quantities is given in Section 4.

Figure 9 plots the perihelion angle φ^{perih} versus A_{in}, the action for the particular set of 26-solar passages corresponding to parabolic motion in the kick region.

3.6. Heuristic outside region action comparsion

Suppose there is a rotational 2-torus $\mathcal{T}^2$. Then it has base $\mathbb{T}^2$ which can be parameterized by (t, φ). Specifying a perihelion fixes a time t^{perih} which leaves one free variable, φ^{perih}. Hence it is possible to make an R-solar passage with any perihelion angle, including the bad angle $\varphi_{\max}^{\text{perih}}$ or some angle near it in the interval of bad angles. Suppose that $\gamma_{\max}$ is a 26-solar passage with perihelion angle $\varphi_{\max}^{\text{perih}}$ (or near it) and initial angular momentum $P_\varphi \approx J_0$ (i.e., nearly parabolic motion). We now describe a procedure to construct γ_{test}, a new curve with smaller action than $\gamma_{\max}$; that is, $A(\gamma_{\text{test}}) < A(\gamma_{\max})$. Doing this completes the proof of the bad angles theorem (Theorem 3.3) since we can take a neighborhood of $\varphi_{\max}^{\text{perih}}$ for the interval of angles specified in the theorem. We may then obtain the necessary contradiction to Lemma 3.1 and rule out the existence of the rotational 2-torus which contains $\gamma_{\max}$.

For $r \geq 5$, ΔH and its derivatives with respect to r and φ are quite small (see Lemma 4.1), so it is not too bad to *approximate the RCP3BP by the 2BP(SC)* for the $(R, 5)$-segment and the $(5, R)$-segments which are contained in the outside region. Doing so allows us to be explicit and compute the action without computer assistance. These approximations are made rigorous in Section 4.

Heuristically, if the comet starts at $R = 26$ and has $\varphi^{\text{perih}} = \varphi_{\text{max}}^{\text{perih}}$, then by modifying the velocity of the $(26, 5)$ segment, the comet can slow down enough so that Jupiter moves from a position where the action is maximized to a position where action is minimized. The comet can then speed very slightly during the $(5, 26)$-segment to arrive at $R = 26$ at the same time as in the original case.

Note that it takes a finite amount of time ΔT for the angle of Jupiter relative to the comet to change by $\Delta \varphi$. In nonrotating coordinates Jupiter moves with unit speed, and for $r \geq 5$ the comet's angle remains nearly constant since $\dot{\psi} = P_{\varphi}/r^2$. (In rotating coordinates, Jupiter is fixed and the comet is moving with almost unit speed.) Hence $\Delta T \approx \Delta \varphi$. By Kepler's second law, for $r \geq 5$ the comet moves slower the further away it is from the Sun (see [AKN]). We denote the amount of time the comet spends in the $(26, 5)$-segment by T_{out}. To keep the argument simple, assume by symmetry; this is also the time spent in the $(5, 26)$-segment.

A very small change in velocity changes considerably the amount of time to reach the perihelion. Let

$$\lambda_{\pm} = \frac{T_{\text{out}}}{T_{\text{out}} \mp \Delta \varphi} \approx \frac{T_{\text{out}}}{T_{\text{out}} \mp \Delta T}. \tag{6}$$

Recall that γ_{max} is a 26-solar passage such that the perihelion angle is $\varphi_{\text{max}}^{\text{perih}}$ and $\gamma_{\text{max}}^{\text{in}}$ *maximizes* action over all 5-solar passages. Consider a new curve γ_{test}, where

- the velocity of the $(26, 5)$-segment is $\dot{\gamma}_{\text{test}}^- = \lambda_- \cdot \dot{\gamma}_{\text{max}}^-$;
- $\gamma_{\text{test}}^{\text{in}}$ is a 5-solar passage which minimizes action over all 5-solar passages; that is, the perihelion angle of γ_{test} is $\varphi_{\text{min}}^{\text{perih}}$;
- the velocity of the $(5, 26)$-segment is $\dot{\gamma}_{\text{test}}^+ = \lambda_+ \cdot \dot{\gamma}_{\text{max}}^+$.

Claim

Suppose that $\gamma \in SP(1.8, 26)$ has initial angular momentum $P_{\varphi} \approx J_0$ (i.e., it is nearly parabolic) and has perihelion angle $\varphi^{\text{perih}} \in [\varphi_{\text{max}}^{\text{perih}} - \Delta, \varphi_{\text{max}}^{\text{perih}} + \Delta]$ for Δ small, for example, $\Delta = 0.000025$. Let γ_{test} be constructed as above. Then $A(\gamma_{\text{max}}) - A(\gamma_{\text{test}}) > 0$ and γ is not a global action minimizer. Let us calculate the difference in actions between γ_{max} and γ_{test}, starting with the action of the rescaled $(26, 5)$-segment γ_{test}^-. The Hamiltonian of the 2BP(SC) approximation for parabolic motion

gives $\langle v, v \rangle / 2 = P_r^2/2 + P_\varphi^2/(2r^2) = 1/r$, where $v = \dot{\gamma}_{\max}$ is the velocity of $\gamma_{\max}$:

$$A(\gamma_{\text{test}}^-) = \int_{t(5) \cdot \lambda_-}^{t(26) \cdot \lambda_-} \left(\frac{\lambda_-^2 \langle v, v \rangle}{2} + \frac{1}{r} \right) \left(\frac{t}{\lambda_-} \right) dt$$

$$= \int_{t(5)}^{t(26)} \lambda_- \cdot \left(\lambda_-^2 \left(\frac{1}{r(u)} \right) + \frac{1}{r(u)} \right) du$$

$$= \int_5^{26} \frac{\lambda_-^3 + \lambda_-}{r\dot{r}} \, dr$$

$$= \int_5^{26} \frac{\lambda_-^3 + \lambda_-}{\sqrt{2r - 1.8^2}} \, dr.$$

Remark. The second line comes from a linear change of variables, and the last line comes from solving $H_{2BP}(r, \varphi, \dot{r}, 1.8) = -1.8$ for $\dot{r}$, as this corresponds to parabolic motion on $\mathcal{S}(1.8)$ The limits of integration change since the comet must start and end at the same place with respect to (r, φ) in the scaled and unscaled cases. By symmetry from the 2BP(SC) approximation, the $(5, R)$-segment γ_{test}^+ is the same computation, only using λ_+. The unscaled trajectories $\gamma_{\max}^+$ and $\gamma_{\max}^-$ have the same computation, only using $\lambda = 1$.

Consider the following formulas relating time and radius for 2BP parabolic motions.

LEMMA 3.4
For parabolic motions in the 2BP,

$$r(t) = \frac{1}{2}(3t + \sqrt{J_0^6 + 9t^2})^{2/3} + \frac{J_0^4}{2(3t + \sqrt{J_0^6 + 9t^2})^{2/3}} - \frac{J_0^2}{2},$$

$$t(r) = \frac{1}{3}\sqrt{2r^3 + 3J_0^2 r^2 - J_0^6}.$$

Proof
These can be derived from formulas in [AKN, Section 2.1].   □

Using the formulas in Lemma 3.4 yields $T_{\text{out}} \approx 60.918$ and

$$\lambda_- \approx 0.9844, \qquad\qquad \lambda_+ \approx 1.0161,$$

$$A(\gamma_{\max}^-) \approx 8.7657, \qquad\qquad A(\gamma_{\max}^+) \approx 8.7657,$$

$$A(\gamma_{\text{test}}^-) \approx 8.4956, \qquad\qquad A(\gamma_{\text{test}}^+) \approx 9.0507.$$

Now let us compute the difference in action between the curves γ_{max} and γ_{test}:

$$A(\gamma_{\text{max}}) - A(\gamma_{\text{test}}) \geq \Delta A_{\text{in}}^{\text{min}} + \left(A(\gamma_{\text{max}}^-) - A(\gamma_{\text{test}}^-)\right) + \left(A(\gamma_{\text{max}}^+) - A(\gamma_{\text{test}}^+)\right)$$

$$\approx 0.000978235 > 0.$$

Further analysis indicates that picking any other radius larger than $R = 26$ also produces a strictly positive result. The reason is that spending more time in the outside region increases T_{out}, which pushes the λ's closer to 1, which makes the differences in action on the $(5, 26)$- and $(26, 5)$-segments smaller and hence increases the difference in actions between γ_{max} and γ_{test}. Hence we conclude that there are no rotational 2-tori corresponding to $R \geq 26$; that is, $e \geq 0.88$.

The next section is dedicated to making the action comparison method mathematically rigorous.

4. Rigorous action comparison

In this section we develop mathematically rigorous estimates to use in place of the heuristics in Section 3. It turns out that by modifying R-solar passages to incorporate elliptic motions, the value of $e^*(0.001, 1.8)$ can be lowered down to $e^* \leq 0.66$ at the cost of increasing complexity of the estimates. This section relies on technical appendices and computer-assisted methods for some of the estimates.

4.1. The intervalization of the RCP3BP

The following formula nicely changes between time and radius:

$$\int_{t_0}^{t_1} dt = \int_{r_0}^{r_1} \frac{dr}{\dot{r}}.$$

Away from parabolic motions,[†] this integral can be rearranged into the form

$$t_1 - t_0 = \int_{r_0}^{r_1} \frac{r\, dr}{\sqrt{2C(r^+ - r)(r - r^-)}}, \tag{7}$$

$$r_+ := \frac{1 + \sqrt{1 - 2C P_\varphi^2}}{2C}, \qquad r_- := \frac{P_\varphi^2}{1 + \sqrt{1 - 2C P_\varphi^2}},$$

$$C := J_0 - P_\varphi + \Delta H.$$

In the case when $\mu = 0$, the integral can be evaluated explicitly since $\Delta H = 0$ and $P_\varphi \equiv P_\varphi(0)$. In the RCP3BP with $\mu > 0$, there are no longer these luxuries, as

[†]Nearly parabolic motions are addressed in Appendix D.

r^+ and r^- are no longer constant; rather, they depend on time. However, away from parabolic motions in the outside region these quantities do not change much since the perturbative effects of Jupiter are too faint to make much of a difference. Our goal is to *intervalize* the problem, that is, to use a computer to generate rigorous bounds on the above terms and to use interval arithmetic (see Appendix A) to manipulate the bounds.

The first step to carrying out this procedure is to get precise estimates on the perturbation terms. Some simple analysis shows the following.

LEMMA 4.1
For $r \geq 1.6$ and $\mu = 10^{-3}$, $|\Delta H| \leq \frac{2.7\mu}{r^3}$, $|\frac{\partial \Delta H}{\partial r}| \leq \frac{12.4\mu}{r^4}$, and $|\frac{\partial \Delta H}{\partial \varphi}| \leq \frac{28.6\mu}{r^3}$.

While these bounds are adequate for exposition, they are not quite accurate enough for our purposes. In Appendix B we define a function $(|\Delta H|)^+(r)$ so that for all $\varphi \in \mathbb{T}$ and $r > 1 + \mu$ it holds that $(|\Delta H|)^+(r) \geq |\Delta H(r, \varphi)|$. Functions $(|\frac{\partial \Delta H}{\partial r}|)^+(r)$ and $(|\frac{\partial \Delta H}{\partial \varphi}|)^+(r)$ are defined similarly.

We also require very accurate estimates on how P_φ changes dynamically with time (or radius). Appendix C contains the construction of a function $\rho(r)$ such that $P_\varphi(t) \in P_\varphi(0) + [-\rho(r(t)), \rho(r(t))]$ for t the time between an apohelion and the following perihelion. Using $\rho(r)$ and some data from rigorous integration (see Section 4.7), one can prove the following lemma.

LEMMA 4.2 (Bounds on change in angular momentum)
Assume $\mu = 10^{-3}$, $J_0 = 1.8$, and $P_\varphi(t) \in [1.66, 1.81]$ (i.e., $e(t) \in [0.48, 1.04]$) for a sufficiently long time interval. Then
(1)   *when approaching a perihelion from the previous apohelion (or from infinity), angular momentum does not change by more than 0.0215298μ over the entire outside region;*
(2)   *when approaching a perihelion from the previous apohelion (or from infinity), angular momentum does not change by more than 4.44885μ;*
(3)   *angular momentum does not change by more than 1.444μ after an R-solar passage.*
    Moreover, by time reversal the same bounds hold when leaving the Sun and are valid until the next apohelion.

Furthermore, one can also prove the following (see Appendix C).

LEMMA 4.3
For $\mu = 10^{-3}$ and $J_0 = 1.8$, then $\rho(r) \leq 18.2\mu/r^3$ for $r \geq 1.6$. Moreover, $\rho(r) \leq 2.7\mu/r^3$ for $r \geq 5$.

This should not come as a great surprise since $P_\varphi(t) - P_\varphi(0) = \int_0^t -(\partial \Delta H)/(\partial \varphi)\, dt$, so angular momentum changes solely due to the perturbation term, which is of order $O(\mu/r^3)$.

4.2. Elongated solar passages

In Section 3.6, we assumed that the $(5, R)$- and $(R, 5)$-segments of an R-solar passage were pieces of the 2BP(SC) corresponding to parabolic motion. This is unnatural for low eccentricity orbits, where the comet does not make large R-solar passages. It is more accurate to use pieces of elliptic orbits. From (6), observe that it is in our favor for the comet to spend as much time as possible in the outside region since $\lambda_\pm \to 1$ as $T_{\text{out}} \to \infty$. By Kepler's second law, the comet moves the slowest, and hence spends the most time near an apohelion (see [AKN]). When constructing the test curve γ_{test}, we exploit this, and instead of using $(5, R)$- and $(R, 5)$-segments, we use elliptic pieces of trajectory which have apohelions. Specifically, start the comet at $r = 5$, advance to an apohelion $r = R$, and move back to $r = 5$. Call this a $(5, R, 5)$-*segment*. Now consider curves γ that decompose into the following (see Figure 10):

- γ^-, a $(5, R_1, 5)$-segment, defined for $t_1 \leq t_5$;
- γ^{in}, a 5-solar passage, defined for $t_5 \leq t_5'$;
- γ^+, a $(5, R_2, 5)$-segment, defined for $t_5' \leq t_2$.

Call these curves *elongated solar passages*. Such curves exist by an argument similar to Lemma 3.2, under the additional assumption that $e(t) \leq 1 - \epsilon$ for some $\epsilon > 0$ for a sufficiently long time interval. This additional condition simply says that to have an elongated solar passage, the comet's eccentricity must stay strictly below $e = 1$ for a long time—enough time—to allow for the existence of the two apohelions. This is a sufficient but not necessary condition, and it can be relaxed slightly; however, it is unnecessary to do so, as the statement Theorem 1.2 only requires $e \leq 0.96$. Existence of elongated solar passages is guaranteed for our purposes by the initial assumptions in Theorem 1.2.

4.3. Asymmetry in the outside region

When approximating the RCP3BP with parabolic motions in Section 3.6 we made use of the fact that the 2BP(SC) approximation of γ^- and γ^+ before and after a 5-solar passage were the same. This is not true in general (see Figure 10). When the comet passes through the kick region, Jupiter changes the angular momentum of the comet. This changes the orbit of the comet in the outside region. In fact, this is the mechanism which allows capture and escape to occur. The change in angular momentum after a 5-solar passage means that the apohelions before and after the 5-solar passage are different; that is, in general, $R_1 \neq R_2$ in an elongated solar passage. This means that γ^- and γ^+ spend different amounts of time in the outside region, and hence λ_- and λ_+ are not directly related.
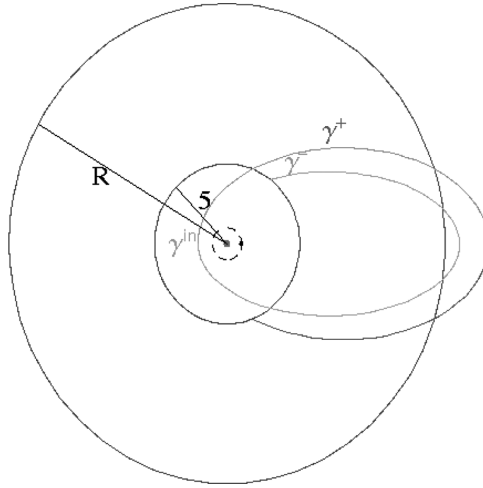
Figure 10. An example of a elongated solar passage

Previously, the case of parabolic motion for the 2BP could be worked out by hand in a short amount of time. The elliptic case involves more complex integrals, and it becomes necessary to use a computer to handle them. The rigorous numerics we use work by integrating intervals of initial conditions (see Appendix A). The integrator only works for shorter intervals of time and is only programmed to handle 5-solar passages. It is enough to handle the estimates in the kick region. The behavior in the outside regions must be accounted for by using a different procedure. We will develop the machinery to overcome both technical difficulties at once.

Consider an elongated solar passage γ, and suppose that the angular momentum satisfies $P_\varphi(t) \in \mathcal{J}_-$ for all $t \in [t_1, t_5]$, that is, where γ^- is defined. Let $P_\varphi(t_5)$ denote the angular momentum at the start of the 5-solar passage γ^{in}, and suppose that $P_\varphi(t_5) \in \mathcal{J}$. The size of the interval $\mathcal{J}$ is ultimately chosen to make the rigorous numerics work efficiently on a computer. Suppose that the angular momentum satisfies $P_\varphi(t) \in \mathcal{J}_+$ for all $t \in [t_5', t_2]$, that is, where γ^+ is defined.

Given $\mathcal{J}$, its possible to derive enclosures for $\mathcal{J}_\pm$ by using Lemma 4.2. For example, to reach the interval $\mathcal{J}$ at time t_5, initial conditions must be contained in $\mathcal{J} + [-2\rho(5), 2\rho(5)] = \mathcal{J}_-$ since this accounts for a change in angular momentum in the outside region. The bound of $2\rho(5)$ is used because the comet passes between $r = 5$ and the apohelion twice, once leaving the Sun, and once approaching it.

Let $(\Delta P_\varphi)_{\text{kick}}(\mathcal{J})$ denote the enclosure of possible changes in angular momentum after passing through the kick region when entering with angular momentum $P_\varphi \in \mathcal{J}$. (This quantity is rigorously estimated in a later subsection.) This means that when leaving the kick region, $P_\varphi \in \mathcal{J} + (\Delta P_\varphi)_{\text{kick}}(\mathcal{J})$. Then when the comet is leaving the

Sun and is in the outside region, $P_\varphi \in \mathcal{J} + (\Delta P_\varphi)_{\text{kick}}(\mathcal{J}) + 2[-\rho(5), \rho(5)] = \mathcal{J}_+$. We remark that for (nonelongated) R-solar passages, the factor of 2 can be removed.

4.4. Bounds on time and radius

We are tasked with estimating all of (7) in detail. Suppose $\mathcal{J} = P_\varphi^* + [-w, w]$ and $|(\Delta P_\varphi)_{\text{kick}}(\mathcal{J})| \leq M$. We call $[-w, w]$ the *window* around P_φ^*. It is an artifact of the rigorous numerics. We use $()^\pm$ to denote upper and lower bounds (see Appendices A, B). Lowercase letters denote values before the 5-solar passage and uppercase letters denote values after the 5-solar passage, respectively. Let

$$c^\pm := J_0 - P_\varphi^* \pm \left(2\rho(5) + w + (|\Delta H|)^+(5)\right),$$

$$C^\pm := J_0 - P_\varphi^* \pm \left(2\rho(5) + w + M + (|\Delta H|)^+(5)\right).$$

Clearly the above quantities bound $C = J_0 - P_\varphi + \Delta H$ before and after a 5-solar passage. (The formal definitions of $(|\Delta H|)^+(r)$ and $\rho(r)$ are found in Appendices B, C, respectively.)

The 2BP(SC) is an integrable system, and specifying Jacobi constant J_0 and P_φ specifies the shape of the ellipse of orbit. Let $2\text{BP}(r_0, \varphi_0; J_0, P_\varphi(0))$ denote the 2BP(SC) with initial conditions (r_0, φ_0), $H_{2BP(SC)} = -J_0$, and $P_\varphi = P_\varphi(0)$. Since $\mu = 10^{-3}$, then the RCP3BP(μ, J_0) with the same initial conditions behaves like $2\text{BP}(r_0, \varphi_0; J_0, P_\varphi(0))$ if r_0 is sufficiently large. For $J_0 = 1.8$ and a given $(r_0, \varphi_0, P_\varphi^*)$, we consider the four special Sun-comet 2BPs with initial conditions $P_\varphi(0) \equiv P_\varphi^* \pm (2\rho(5) + w)$, $P_\varphi(0) \equiv P_\varphi^* \pm (2\rho(5) + w + M)$. Call the 2BPs with these angular momenta the *extreme 2BPs* with respect to P_φ^*. We use them to approximate the RCP3BP far from the Sun.

Consider an elongated solar passage γ of the RCP3BP with angular momentum $P_\varphi(t_5) \in \mathcal{J} = P_\varphi^* + [-w, w]$ at the start of a 5-solar passage. Then for $t \in [t_1, t_5]$, γ has $P_\varphi(t) \in P_\varphi^* \pm (2\rho(5) + w)$. This is to say that the angular momentum in the RCP3BP is bounded in between that of the extreme 2BPs with $P_\varphi(0) \equiv P_\varphi^* \pm (2\rho(5) + w)$ in the outside region. A similar statement can be made about times $t \in [t_5', t_2]$.

Examination of (7) indicates that by bounding P_φ, a bound on the time spent in the outside region may also be obtained. Moreover, once bounds on time are obtained, these can be used to obtain bounds on the action in the outside region. Hence to carry out the action comparison rigorously using the elongated solar passages for RCP3BP, it suffices to do it by using extreme 2BP approximations in the outside region. The values of action for RCP3BP are contained within the range of values obtained by performing the action comparison using extreme 2BPs.

For small w it follows from Lemma 4.2 that the range of angular momenta is not more than 3μ between the extreme 2BPs, so in the outside region away from parabolic motions ($e \leq 0.96$), there is no qualitative difference from using the extreme 2BP approximations. We select w large enough to be amenable to our rigorous numerics, but not so large as to introduce qualitatively different phenomenon. For nearly parabolic motions $e > 0.96$, then a similar analysis holds if we use extreme 2BP approximations of R-solar passages.

In light of the integrals in Appendix D, note that for the 2BP(SC), the time from the apohelion to $r = 5$ is given by

$$T_{\text{out}} = \frac{I_1(r_-, r_+, 5, r_+)}{\sqrt{2(J_0 - P_\varphi)}},$$

where r_- and r_+ are given in (7). For the RCP3BP, these quantities can be estimated as

$$r_-^\pm := \frac{(P_\varphi^* \pm 2\rho(5) \pm w)^2}{1 + \sqrt{1 - 2(c^\pm)(P_\varphi^* \pm 2\rho(5) \pm w)^2}},$$

$$r_+^\pm := \frac{1 + \sqrt{1 - 2(c^\mp)(P_\varphi^* \mp 2\rho(5) \mp w)^2}}{2(c^\mp)},$$

$$R_-^\pm := \frac{(P_\varphi^* \pm 2\rho(5) \pm w \pm M)^2}{1 + \sqrt{1 - 2(C^\pm)(P_\varphi^* \pm 2\rho(5) \pm w)^2}},$$

$$R_+^\pm := \frac{1 + \sqrt{1 - 2(C^\mp)(P_\varphi^* \mp 2\rho(5) \mp w \mp M)^2}}{2(C^\mp)}.$$

Remarks on notation
All of these quantities are functions of P_φ^*, w, M, and J_0; however, we adopt the above notation for brevity. Note that lower bounds are denoted $()^-$, upper bounds are denoted $()^+$, and the subscripts $()_\pm$ indicate different extreme 2BPs. Furthermore, when reading the expressions, note that $x^\pm = a \pm b \pm c$ means $x^\pm = a \pm (b + c)$; that is, specifying a sign choice on the left-hand side specifies all choices on the right-hand side. This notation avoids overuse of parentheses. Conceptually, one should think of such expressions as intervals. For example, to understand $(P_\varphi^* \pm 2\rho(5) \pm w \pm M)$, it is easier to think of it as some bound on $P_\varphi(t)$ over some range of time.

For RCP3BP, we let $t_{\text{out}} = t_5 - t_1$ be the time γ^- spends in the outside region, that is, the time spent from initial conditions until the start of 5-solar passage. Let $T_{\text{out}} = t_2 - t_5'$ be the time γ^+ spends in the outside region, that is, the time spent from

the end of 5-solar passage until the final conditions. These times will be estimated shortly.

Let us use the estimates on P_φ, ΔH, r^{perih}, and r^{apoh} to estimate quantities in the action comparison. Define

$$b_{\text{out}}^\pm(k) := \frac{I_k(r_-^\pm, r_+^\mp, 5, r_+^\mp)}{\sqrt{2(c^\mp)}}, \qquad B_{\text{out}}^\pm(k) := \frac{I_k(R_-^\pm, R_+^\mp, 5, R_+^\mp)}{\sqrt{2(C^\mp)}},$$

where the I_k are integrals defined in Appendix D. The signs of $()_\pm^\pm$ are chosen so that they are all consistent with using a single extreme 2BP for each of the four possible bounds $b_{\text{out}}^\pm$, $B_{\text{out}}^\pm$. It follows that $t_{\text{out}} \in 2[b_{\text{out}}^-(1), b_{\text{out}}^+(1)]$ and $T_{\text{out}} \in 2[B_{\text{out}}^-(1), B_{\text{out}}^+(1)]$. The factor of 2 comes from the fact that the distance from $r = 5$ to an apohelion is traversed twice in an elongated solar passage. The other values of k are used later. In the case of an R-solar passage, the factor of 2 can be removed.

4.5. λ-estimates

If $(r(t), \varphi(t), \dot{r}(t), \dot{\varphi}(t))$ is a solution to the Euler-Lagrange equations, then the rescaled trajectory

$$\left(r\left(\frac{t}{\lambda}\right), \varphi\left(\frac{t}{\lambda}\right), \lambda\dot{r}\left(\frac{t}{\lambda}\right), \lambda\dot{\varphi}\left(\frac{t}{\lambda}\right)\right) = \left(r_\lambda(t), \varphi_\lambda(t), \dot{r}_\lambda(t), \dot{\varphi}_\lambda(t)\right)$$

is also a solution to the Euler-Lagrange equations. The equations of motion give

$$\dot{\varphi} = -1 + \frac{P_\varphi}{r^2}, \qquad \dot{\varphi}_\lambda = \left(-1 + \frac{P_\varphi}{r^2}\right)\lambda.$$

Hence

$$\varphi(t) = \varphi(0) - t + \int_0^t \frac{P_\varphi(s)}{r(s)^2}\, ds, \qquad \varphi_\lambda(t) = \varphi(0) - \lambda t + \lambda \int_0^t \frac{P_\varphi(s)}{r(s)^2}\, ds.$$

Now compute the differences in angle over time, and solve for λ to get

$$\lambda(t) = 1 - \frac{\varphi_\lambda(t) - \varphi(t)}{t - \int_0^t (P_\varphi(s))/(r^2(s))\, ds}. \tag{8}$$

We need to use this formula as opposed to (6) since it explicitly uses the motion of the comet in the rotating frame, whereas (6) made the approximation that the comet rotates with speed 2π (equivalently not at all in the fixed frame). This is not necessarily a big difference in the outside region but nonetheless must be justified. Formula (8) can be interpreted as telling us how much of a rescaling λ is needed if we specify the

difference $\Delta\varphi = (\varphi_\lambda(t) - \varphi(t))$ of angles from the rescaled and original trajectories at time t. Note that when using (8), it is more convenient to calculate the difference in angles at the start of the 5-solar passage γ^{in} since then estimates of λ require only data about the outside region. Define the angles $\varphi_{\max}^{t_5}(P_\varphi)$ and $\varphi_{\min}^{t_5}(P_\varphi)$ such that

$$A_{\text{in}}\big(P_\varphi, \varphi_{\max}^{t_5}(P_\varphi)\big) := \max_\gamma A(\gamma^{\text{in}}), \qquad A_{\text{in}}\big(P_\varphi, \varphi_{\min}^{t_5}(P_\varphi)\big) := \min_\gamma A(\gamma^{\text{in}}),$$

where the minimum and maximum are taken over all elongated solar passages on the energy surface $\mathcal{S}(J_0)$ with angular momentum $P_\varphi(t_5) = P_\varphi$ at the start of the 5-solar passage (cf. (4)). Now let us compute the difference in action and angle with respect to an interval of initial conditions (cf. (5)):

$$\Delta A_{\text{in}}^{\min}(\mathcal{J}) := \min_{P_\varphi \in \mathcal{J}} \big(A_{\text{in}}(P_\varphi, \varphi_{\max}^{t_5}(P_\varphi)) - A_{\text{in}}(P_\varphi, \varphi_{\min}^{t_5}(P_\varphi))\big),$$

$$\Delta\varphi^{t_5}(\mathcal{J}) := \varphi_{\max}^{t_5}(\mathcal{J}) - \varphi_{\min}^{t_5}(\mathcal{J}).$$

As defined, $\Delta\varphi(\mathcal{J})$ is an interval, and methods to enclose it are developed shortly. Using $\Delta\varphi^{t_5}$ is acceptable since this new difference in angles with the newly defined minimal and maximal angles flows into solutions with perihelion angles which minimize or maximize action. Hence the bad angles theorem still applies. Our test curve γ_{test} is constructed as in Section 3.6 by means of slowing down on γ_{test}^-, making a cheaper 5-solar passage on $\gamma_{\text{test}}^{\text{in}}$, and speeding up on γ_{test}^+.

Now let us estimate $\lambda_\pm$ by using each of the extreme 2BPs listed in Section 4.4. First estimate

$$\int_0^t \frac{P_\varphi(s)}{r^2(s)}\,ds = \int_{r(0)}^{r(t)} \frac{dr}{\dot{r}r^2} = \int_{r_0}^{r_1} \frac{P_\varphi\,dr}{\sqrt{2(J_0 - P_\varphi + \Delta H)r(r^{\text{apoh}} - r)(r - r^{\text{perih}})}},$$

which for motions away from $e = 1$ looks like the integral I_{-1} from Appendix D multiplied by P_φ. Let

$$d := [(P_\varphi^* - 2\rho(5) - w) \cdot b_{\text{out}}^-(-1), (P_\varphi^* + 2\rho(5) + w) \cdot b_{\text{out}}^+(-1)],$$

$$D := [(P_\varphi^* - 2\rho(5) - w - M) \cdot B_{\text{out}}^-(-1), (P_\varphi^* + 2\rho(5) + w + M) \cdot B_{\text{out}}^+(-1)].$$

Let $\lambda_\pm(\mathcal{J})$ denote the interval of scalings $\lambda_\pm$ needed to construct the test curves γ_{test} corresponding to $\gamma_{\max}$, an elongated solar passage with perihelion angle $\varphi_{\max}^{\text{perih}}$ and $P_\varphi(t_5) \in \mathcal{J}$. Then let

$$\lambda_-^\pm(\mathcal{J}) := 1 - \frac{(\Delta\varphi(t_5))(\mathcal{J})}{2\big([b_{\text{out}}^-(1), b_{\text{out}}^+(1)] - d\big)},$$

$$\lambda_+^\pm(\mathcal{J}) := 1 + \frac{(\Delta\varphi(t_5))(\mathcal{J})}{2\big([B_{\text{out}}^-(1), B_{\text{out}}^+(1)] - D\big)}.$$

The signs in $\lambda_\pm^\pm$ come about by examining the action comparison in the kick region and noting that the angle corresponding to maximal action comes after the angle corresponding to the minimal action; that is, it is less than π to the right of $\varphi_{\min}^{\text{perih}}$ and more than π to the left on the circle (see Figure 9). Then starting at the maximal action, we need a slower moving comet; that is, we need $\lambda_- < 1$. Thinking of this another way, since $\dot\varphi < 0$, slowing down means spending more time in the outside region, which means that φ decreases. We remark that the factor of 2 in the denominator can be removed when considering R-solar passages.

4.6. Action decomposition

Using $H = -J_0$, it follows that for elliptic motions, $\langle v, v \rangle/2 = P_r^2/2 + P_\varphi^2/(2r^2) = 1/r - \Delta H - J_0 + P_\varphi$, where $v = \dot\gamma_{\max}$. The rescaled action for the elliptic case is

$$
\begin{aligned}
A(\lambda, t_0, t_1) &= \int_{t_0\lambda}^{t_1\lambda} \left(\frac{\lambda^2 \langle v, v \rangle}{2} + \frac{1}{r} - \Delta H \right) \left(\frac{t}{\lambda} \right) dt \\
&= \lambda \int_{t_0}^{t_1} \left(\lambda^2 \left(\frac{1}{r} - \Delta H - J_0 + P_\varphi \right) + \frac{1}{r} - \Delta H \right)(u) \, du \\
&= \int_{t_0}^{t_1} \frac{\lambda^3 + \lambda}{r} \, dt + \int_{t_0}^{t_1} \lambda^3 (-J_0 + P_\varphi) \, dt + \int_{t_0}^{t_1} (\lambda^3 + \lambda)(-\Delta H) \, dt.
\end{aligned}
$$

Define

$$
A_P(\lambda, t_0, t_1) := \int_{t_0}^{t_1} \frac{\lambda^3 + \lambda}{r} \, dt,
$$

$$
A_K(\lambda, t_0, t_1) := \int_{t_0}^{t_1} \lambda^3 (-J_0 + P_\varphi) \, dt,
$$

$$
A_{\Delta H}(\lambda, t_0, t_1) := \int_{t_0}^{t_1} (\lambda^3 + \lambda)(-\Delta H) \, dt,
$$

so that $A = A_P + A_K + A_{\Delta H}$. To do the action comparison one must estimate

$$
\begin{aligned}
A(1, t_{\text{out}}) &- A(\lambda_-, t_{\text{out}}) + A(1, T_{\text{out}}) - A(\lambda_+, T_{\text{out}}) \\
&= A_P(1, t_{\text{out}}) - A_P(\lambda_-, t_{\text{out}}) + A_P(1, T_{\text{out}}) - A_P(\lambda_+, T_{\text{out}}) \\
&\quad + A_K(1, t_{\text{out}}) - A_K(\lambda_-, t_{\text{out}}) + A_K(1, T_{\text{out}}) - A_K(\lambda_+, T_{\text{out}}) \\
&\quad + A_{\Delta H}(1, t_{\text{out}}) - A_{\Delta H}(\lambda_-, t_{\text{out}}) + A_{\Delta H}(1, T_{\text{out}}) - A_{\Delta H}(\lambda_+, T_{\text{out}}).
\end{aligned}
$$

To estimate each of these terms, our strategy is to get lower and upper bounds by using the extreme 2BPs.

4.6.1. -$A_{\Delta H}$ estimates

$$A_{\Delta H}(1, t_{out}) - A_{\Delta H}(\lambda_-, t_{out}) + A_{\Delta H}(1, T_{out}) - A_{\Delta H}(\lambda_+, T_{out})$$

$$= \int_{t_{out}} (2 - \lambda_-^3 - \lambda_-)(-\Delta H)\, dt + \int_{T_{out}} (2 - \lambda_+^3 - \lambda_+)(-\Delta H)\, dt$$

$$\in 2[b_{out}^-(1), b_{out}^+(1)](2 - [\lambda_-^-, \lambda_-^+]^3 - [\lambda_-^-, \lambda_-^+]) \cdot (|\Delta H|)^+(5)[-1, 1]$$

$$+ 2[B_{out}^-(1), B_{out}^+(1)](2 - [\lambda_+^-, \lambda_+^+]^3 - [\lambda_+^-, \lambda_+^+]) \cdot (|\Delta H|)^+(5)[-1, 1].$$

This term is small, usually of the order $10\mu^2$, and no additional refinements need to be made to this estimate.

4.6.2. -A_K estimates
Let us estimate

$$A_K(1, t_{out}) - A_K(\lambda_-, t_{out}) + A_K(1, T_{out}) - A_K(\lambda_+, T_{out})$$

$$= \int_{t_{out}} \left(1 - \lambda_-^3\right)(-J_0 + P_\varphi)\, dt + \int_{T_{out}} \left(1 - \lambda_+^3\right)(-J_0 + P_\varphi)\, dt$$

using the extreme 2BPs. To keep notation simple, let $\min(\mathcal{J}_-) = m_-$, let $\max(\mathcal{J}_-) = m_+$, let $\min(\mathcal{J}_-) = M_-$, and let $\max(\mathcal{J}_+) = M_+$:

$$\int_{t_{out}} (1 - \lambda_-^3)(-J_0 + P_\varphi)\, dt + \int_{T_{out}} (1 - \lambda_+^3)(-J_0 + P_\varphi)\, dt$$

$$\subset 2\big[(b_{out}^-(1)) \cdot (1 - (\lambda_-^-)^3) \cdot (-J_0 + m_-), (b_{out}^+(1)) \cdot (1 - (\lambda_-^+)^3) \cdot (-J_0 + m_+)\big]$$

$$+ 2\big[(B_{out}^-(1)) \cdot (1-(\lambda_+^+)^3) \cdot (-J_0+M_-), (B_{out}^+(1)) \cdot (1-(\lambda_+^-)^3) \cdot (-J_0 + M_+)\big].$$

Note the logic of the interval bounds. For example, $b_{out}^-(1)$ is paired with λ_-^- and m_- since smaller angular momentum means a smaller apohelion, meaning less time is spent in the outer region; that is, a smaller t_{out} and less time in the outside region means a worse λ-value, that is, farther from one, that is, a smaller $\lambda_- < 1$. The logic for the other pairings is similar.

4.6.3. -A_P estimates
Now estimate

$$A_P(1, t_{out}) - A_P(\lambda_-, t_{out}) + A_P(1, T_{out}) - A_P(\lambda_+, T_{out})$$

$$= \int_{t_{out}} \frac{2 - (\lambda_-^3 + \lambda_-)}{r}\, dt + \int_{T_{out}} \frac{2 - (\lambda_+^3 + \lambda_+)}{r}\, dt$$

by using the extreme 2BPs. Note that these integrals look like I_0 from Appendix D after appropriate change of variables. To keep notation simple, let $\min(\mathcal{J}_-) = m_-$, let $\max(\mathcal{J}_-) = m_+$, let $\min(\mathcal{J}_-) = M_-$, and let $\max(\mathcal{J}_+) = M_+$:

$$
\int_{t_{\text{out}}} \frac{2 - (\lambda_-^3 + \lambda_-)}{r} \, dt + \int_{T_{\text{out}}} \frac{2 - (\lambda_+^3 + \lambda_+)}{r} \, dt
$$
$$
\subset 2\big[(b_{\text{out}}^-(0)) \cdot (2 - (\lambda_-^-)^3 - \lambda_-^-), (b_{\text{out}}^+(0)) \cdot (2 - (\lambda_-^+)^3 - \lambda_-^+)\big]
$$
$$
+ 2\big[(B_{\text{out}}^+(0)) \cdot (2 - (\lambda_+^-)^3 - \lambda_+^-), (B_{\text{out}}^-(0)) \cdot (2 - (\lambda_+^+)^3 - \lambda_+^+)\big].
$$

Remark. The bounds for A_P, A_K, and $A_{\Delta H}$ are readily computable on a computer. It is fairly easy to develop formulas to handle the action comparison for nearly parabolic motions by using standard R-solar passages. After some initial setup, the formulas from this section remain almost unchanged (see Appendix D.1 for details).

4.7. Rigorous computation of action in the kick region

In this subsection we consider $\mu = 10^{-3}$ and $J_0 = 1.8$ and develop precise estimates on how action varies in the kick region. We program the computer-aided process design (CAPD) package to rigorously integrate trajectories over 5-solar passages and record $\Delta A_{\text{in}}^{\min}(\mathcal{J})$, $\Delta\varphi^{t_5}(\mathcal{J})$, $(\Delta P_\varphi)_{\text{kick}}(\mathcal{J})$, and the time to cross the kick region.

THEOREM 4.4
For RCP3BP(0.001, 1.8) and $P_\varphi \in [1.6875, 1.81]$, that is, for $e \in [0.6, 1.03]$,

$$
\Delta A_{\text{in}}^{\min}([1.6875, 1.81]) \geq 15.9748\mu,
$$
$$
\Delta\varphi^{t_5}([1.6875, 1.81]) \leq 1.2495,
$$
$$
|(\Delta P_\varphi)_{\text{kick}}([1.6875, 1.81])| \leq 1.40093\mu.
$$

Furthermore, for $P_\varphi \in [1.71, 1.81]$, the maximum time to cross the kick region is less than 19.5256 *time units, that is, approximately three revolutions of Jupiter.*

Proof
We program the CAPD package to rigorously integrate trajectories over a 5-solar passage. The CAPD package makes use of interval arithmetic to enclosure numerical solutions of ODEs over short periods of time in rigorously verified ϵ-tubes. It is also capable of moving small boxes of initial conditions under the flow. By covering a domain with many small intervals, CAPD can move the entire domain (see Appendices A, F for more details on CAPD and interval arithmetic).

We note that action can also be simultaneously solved when computing the solution to an ODE by noting that since action is the integral of the Lagrangian (3) that is, $A(t) = \int_0^t L(s)\,ds$, then $\dot{A} = L(t)$, and $L(t)$ depends only on the polar variables at time t, which are known after one step of the integrator.

For each 5-solar passage, use initial conditions $A(0) = 0$, $r = 5$, $P_\varphi \in [1.6875, 1.81]$, $\varphi \in \mathbb{T}$. Subdivide $[1.6875, 1.81]$ into 4901 boxes of size 0.000025, and subdivide $[-\pi, \pi]$ into 12567 boxes of size 0.000025. Use the implicit definition of $P_r = \sqrt{2(1.8 - (P_\varphi^2)/(2r^2) + 2/r - \Delta H(r, \varphi))}$ on the energy surface $\mathcal{S}(1.8)$.

Use CAPD with a 5th-order Taylor method and adaptive time-step sizes of $h \leq 0.1$ to rigorously integrate trajectories until they cross $\{r = 5\}$ again. Record the action before and after the box of trajectories crosses $\{r = 5\}$. Then make an interval out of the lower and upper bounds on action while crossing. Since the box is small, with the use of adaptive step size, the width of the action interval is small, and it accurately measures action for the box of initial conditions being integrated over the 5-solar passage. We do this for each trajectory with a fixed box of P_φ's, that is, for $P_\varphi(t_5) \in P_\varphi^* + [-w, w] = \mathcal{I}$ with $w = 0.0000125$ and $P_\varphi^* = 1.6875 + 0.000025k$, $k = 0, \ldots, 4901$. In this fashion the interval $P_\varphi \in [1.6875, 1.81]$ is covered. The action difference for each k is bounded using the largest lower bound of all the action intervals and the smallest upper bound. Actual differences could be larger. Also recorded is the angle of the initial conditions, which produces each extremal box, the maximum change in angular momentum for each window of initial condition $\mathcal{I}$, and the exit times.

This all gives the data in the statement of the theorem. Note that this method actually produces an extensive list of boxes and bounds. For each P_φ, there is a picture like Figure 9. The differences in action are plotted in Figure 11.   □

Remark. This setup is expensive and took 15 computers 2 weeks to complete the comparison. Fortunately the integration of each box of initial conditions is independent of the others, and the problem naturally lends itself to parallel computation. The programs and data for this procedure are available upon request (see Appendix F). We also remark that choice of parameters can affect bounds obtained and running time. For our choice of parameters, the integration time needed to cross the kick region is small, less than 19.5256 time units. For the $\mu = 0.001$ and $J_0 \geq 1.52$, the CAPD integrator works well for the RCP3BP over short time intervals, say, for less than 50 time units. However, for more lengthy integrations, additional work is needed to validate the behavior of a solution. In [GK2] we present a method for long time integration.

Using the above estimates for the outside region, as well as the rigorous integration data for the kick region, a program was written to compare action. The result is the
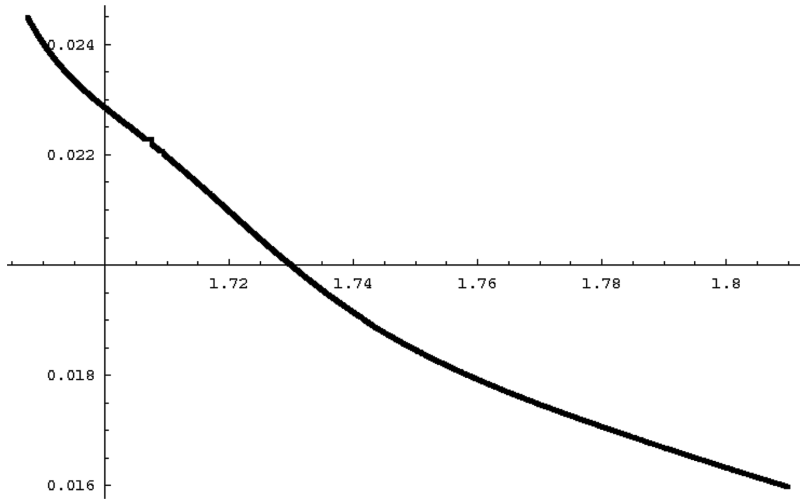
Figure 11. Lower bounds on $\Delta A_{\mathrm{in}}^{\min}(P_\varphi)$ versus P_φ

estimate in the main theorem that $e^*(0.001, 1.8) \leq 0.66$. The software is general enough to handle other values of μ and J_0.

The next several sections of the paper are dedicated to analysis of the map $\mathscr{F}_\mu$.

5. Delaunay variables

For the 2BP there is a natural well-defined action angle coordinate system known as *Delaunay variables*. A derivation of Delaunay variables is found in [GPS] (see also [AKN], [CC] for some nice exposition). In short, they arise by considering the generating function

$$S(r, \varphi, L, G) = \varphi G + \int_{r^{\mathrm{perih}}(L,G)}^{r} \left(\sqrt{\frac{-1}{L^2} - \frac{G^2}{r^2} + \frac{2}{r}} \right) dr.$$

This gives the canonical transformation $\mathcal{D}(\ell, g, L, G) = (r, \varphi, P_r, P_\varphi)$ from Delaunay variables to symplectic polar variables, where $r^{\mathrm{perih}} = L^2(1 - \sqrt{1 - G^2/L^2})$ is the perihelion of the 2BP(SC) expressed in terms of L, G. The image of $\mathcal{D}$ is only defined for bounded motions of the 2BP(SC) with $(\ell, g) \in \mathbb{T}^2$ and $0 \leq G \leq L$.

For the 2BP, L^2 is the semimajor axis of the ellipse of the orbit, so by Kepler's third law, the period $T = 2\pi L^3$. Upon examination of the generating function, observe that $G = P_\varphi$ is *angular momentum*, or alternatively LG is the semiminor axis of the ellipse of the orbit. The variable $\ell \in \mathbb{T}$ is the *mean anomaly* which is $\ell = \pi \mod 2\pi$ at the apohelion, $\ell = 0 \mod 2\pi$ at the perihelion, and in general $(\ell - \ell_0) = 2\pi / T t$. The quantity $(g + t)$ can be interpreted as the perihelion angle. (In nonrotating coordinates g itself plays this role.) It is possible to recover radius from Delaunay coordinates by

noting that $r = L^2(1 - e\cos(u))$, where the eccentricity $e = \sqrt{1 - G^2/L^2}$, and u, *the mean anomaly*, is given implicitly by the *Kepler equation* $u - e\sin(u) = \ell$.

Applying the canonical transformation $\mathcal{D}$ to the Hamiltonian for the 2BP(SC) in rotating polar coordinates gives

$$H_{2BP(SC)} \circ \mathcal{D}^{-1} = -\frac{1}{2L^2} - G.$$

Note that S satisfies $\det(\frac{\partial^2 S}{\partial(r,\phi)\partial(L,G)}) = \frac{L^3}{P_r} \neq 0$. Hence in general there exists a canonical transformation from polar to Delaunay, provided the generating function is well defined (see [AKN]). Hence where it makes sense, one gets Delaunay variables for RCP3BP by using the generating function S. This yields

$$H_{\text{Del}} = H_{\text{Polar}} \circ \mathcal{D}^{-1} = -\frac{1}{2L^2} - G + \Delta H(L, G, \ell, g), \qquad (9)$$

where the perturbation term is converted to Delaunay. As the "where it makes sense" indicates, Delaunay variables are not defined for the RCP3BP for nearly parabolic motions. In [GK1] we develop techniques to overcome this limitation.

6. Twisting in Delaunay coordinates

Consider the Poincaré section $\Gamma = \{g = 0 \mod 2\pi\} \subset \mathcal{S}(J_0)$. In Section B.2 we show that $-1.025 \leq \dot{g} \leq -0.9975$ for $J_0 = 1.8$ and $\mu \leq 10^{-3}$, and hence Γ is well defined. Consider the Poincaré return map $\mathcal{F} : \mathcal{S}^{\text{out}}(J_0) \cap \Gamma \mapsto \mathcal{S}^{\text{out}}(J_0) \cap \Gamma$ defined by

$$\mathcal{F} = \mathcal{F}_{\mu,J_0} : (\ell_0, L_0) \mapsto (\ell_1, L_1) = \big(\ell(t_\Gamma, \ell_0, L_0), L(t_\Gamma, \ell_0, L_0)\big), \qquad (10)$$

where $t_\Gamma > 0$ is the first return time to Γ. In this section, we show that in Delaunay coordinates, the return map $\mathcal{F}$ is an EAPT map for $L \in [L_{\text{twist}}^-(\mu, J_0), L_{\text{twist}}^+(\mu, J_0)]$ (see [MF], [B], [G], [Mo1], [S] for exposition on EAPT maps). Numerically a computer can find $[1.611, 15.94] \subset [L_{\text{twist}}^-(0.001, 1.8), L_{\text{twist}}^+(0.001, 1.8)]$. This translates into $[0.07, 0.994] \subset [e_{\text{twist}}^-(0.001, 1.8), e_{\text{twist}}^+(0.001, 1.8)]$ and gives the twist region Tw^{Del}.

6.1. Twisting conditions

Our goal is to develop an explicit condition which can be numerically checked to verify twist. The energy reduction formulas found in Appendix E.2 allow us to write an autonomous Hamiltonian system as a time-dependent Hamiltonian. Following the construction for 2 degrees of freedom, fix μ and J_0 so that $H = -J_0$ (i.e., restrict dynamics to $\mathcal{S}(J_0)$), and write $G = G(L, \ell, g, J_0)$ implicitly in terms of the others variables. The construction in Appendix E.2 produces a time-dependent Hamiltonian

$\tilde{H}_{J_0}(L, \ell, \tilde{t})$, where $\tilde{t} = g$ is now the time variable. The construction is well defined since $\dot{g} = -1 + \frac{\partial \Delta H}{\partial G} = -1 + O(\frac{\mu}{L^6}) < 0$ for μ small. Furthermore, from the construction, one can compute

$$\frac{\partial}{\partial L} \tilde{H}_{J_0}(L, \ell, \tilde{t}) = \frac{\left(\frac{\partial H(L,\ell,g,G(L,\ell,g,J_0))}{\partial L} \right)}{\left(\frac{\partial H(L,\ell,g,G(L,\ell,g,J_0))}{\partial G} \right)}.$$

Now look at the second derivative with respect to L:

$$\frac{\partial}{\partial L} \left(\frac{\partial \tilde{H}_{J_0}(L, \ell, \tilde{t})}{\partial L} \right) = \frac{\partial}{\partial L} \left(\frac{\left(\frac{\partial H(L,\ell,g,G(L,\ell,g,J_0))}{\partial L} \right)}{\left(\frac{\partial H(L,\ell,g,G(L,\ell,g,J_0))}{\partial G} \right)} \right)$$

$$= \frac{1}{\frac{\partial H}{\partial G}} \frac{\partial}{\partial L} \left(\frac{\partial H}{\partial L} (L, \ell, g, G(L, \ell, g, J_0)) \right)$$

$$- \left(\frac{\partial H}{\partial L} \right) \left(\frac{1}{(\frac{\partial H}{\partial G})^2} \right) \frac{\partial}{\partial L} \left(\frac{\partial H}{\partial G} (L, \ell, g, G(L, \ell, g, J_0)) \right)$$

$$= \frac{\left(\frac{\partial H}{\partial G} \right) \left(\frac{\partial^2 H}{\partial L^2} + \frac{\partial^2 H}{\partial L \partial G} \frac{\partial G}{\partial L} \right) - \left(\frac{\partial H}{\partial L} \right) \left(\frac{\partial^2 H}{\partial L \partial G} + \frac{\partial^2 H}{\partial G^2} \frac{\partial G}{\partial L} \right)}{(\frac{\partial H}{\partial G})^2}.$$

There is a $\frac{\partial G}{\partial L}$ to be dealt with. From the Hamiltonian (9), G is implicitly defined by

$$G = J_0 - \frac{1}{2L^2} + \Delta H \big(L, \ell, g, G(J_0, L, \ell, g) \big).$$

Differentiate this expression to obtain

$$\frac{\partial G}{\partial L} = L^{-3} + \left(\frac{\partial \Delta H}{\partial L} \right) + \left(\frac{\partial \Delta H}{\partial G} \right) \left(\frac{\partial G}{\partial L} \right),$$

and solve to find

$$\frac{\partial G}{\partial L} = \frac{L^{-3} + \left(\frac{\partial \Delta H}{\partial L} \right)}{1 - \left(\frac{\partial \Delta H}{\partial G} \right)}.$$

One can now compute the partial derivatives of H and plug everything into the above expression for $\frac{\partial}{\partial L} \left(\frac{\partial \tilde{H}_{J_0}(L, \ell, \tilde{t})}{\partial L} \right)$. With the aid of a computer it is possible to estimate this term, which we call the *twist term*. Let us examine why this derivative is so important now.

6.2. Proof of EAPT for the return map $\mathcal{F}$

Since $\mathcal{F}$ arises as the Poincaré return map of an autonomous 2 degrees of freedom Hamiltonian, it is exact and area preserving. The twist condition for $\mathcal{F}$ is equivalent to $\frac{\partial \ell_1}{\partial L_0} = \frac{\partial \ell(t_\Gamma, \ell_0, L_0)}{\partial L_0} < 0$ (see [B], [MF]).

Claim

Note that $\frac{\partial}{\partial L}\left(\frac{\partial \tilde{H}_{J_0}(L,\ell,\tilde{t})}{\partial L}\right)$ is of constant sign in a domain Ω if and only if $\mathcal{F}_\mu$ is an EAPT in Ω.

Proof

Let us consider the equations of first variation

$$
\frac{d}{d\tilde{t}}\begin{pmatrix} \frac{\partial \ell}{\partial \ell_0} & \frac{\partial \ell}{\partial L_0} \\ \frac{\partial L}{\partial \ell_0} & \frac{\partial L}{\partial L_0} \end{pmatrix} = \begin{pmatrix} \frac{\partial^2 \tilde{H}_{J_0}}{\partial \ell \partial L} & \frac{\partial^2 \tilde{H}_{J_0}}{\partial L^2} \\ -\frac{\partial^2 \tilde{H}_{J_0}}{\partial \ell^2} & -\frac{\partial^2 \tilde{H}_{J_0}}{\partial \ell \partial L} \end{pmatrix}\begin{pmatrix} \frac{\partial \ell}{\partial \ell_0} & \frac{\partial \ell}{\partial L_0} \\ \frac{\partial L}{\partial \ell_0} & \frac{\partial L}{\partial L_0} \end{pmatrix}.
$$

In particular, at time $\tilde{t} = 0$ it holds that

$$
\frac{d}{d\tilde{t}}\left(\frac{\partial \ell}{\partial L_0}\right)\Big|_{\tilde{t}=0} = \frac{\partial^2 \tilde{H}_{J_0}}{\partial L^2}\Big|_{\tilde{t}=0}.
$$

Hence the sign of $\frac{\partial^2 \tilde{H}_{J_0}}{\partial L^2}|_{\tilde{t}=0}$ determines whether $\frac{\partial \ell}{\partial L_0}$ is decreasing or increasing near $\tilde{t} = 0$. But $\frac{\partial \ell}{\partial L_0}|_{\tilde{t}=0} = 0$, so the sign of $\frac{\partial^2 \tilde{H}_{J_0}}{\partial L^2}$ determines the sign of $\frac{\partial \ell}{\partial L_0}\big|_{\tilde{t}=0}$ in a neighborhood of $\tilde{t} = 0$; that is, it determines twist for the flow over a small increment of time. So if $\text{sign}\left(\frac{\partial^2 \tilde{H}_{J_0}}{\partial L^2}\right)$ is constant for all $\tilde{t} \in [0, 2\pi]$, $\ell_0 \in \mathbb{T}$, and L_0 in some interval, then the map $\mathcal{F}$ is twisting in that region.

The above argument shows that the time-ϵ map for some small ϵ of the flow is a twist map. In [GK2], we develop a method to prove that in fact the map $\mathcal{F}_\mu$ is a twist map as defined above, using $\Gamma = \{g = 0 \mod 2\pi\}$ (that is, for $\epsilon = 2\pi$). The technique involves globally estimating and solving (with computer assistance) the equations of first variation. The key to this method is a geometric formulation of twisting in polar variables which allows one to deduce results from the much more managable equations of first variation in polar coordinates. $\qquad\square$

In the case $\mu = 0$, the twist term satisfies $\frac{\partial \ell_1}{\partial L_0} = -\frac{3}{L_0^4} \cdot 2\pi < 0$. Then for $\mu > 0$ it is natural to require $\frac{\partial \ell_1}{\partial L_0} = -\frac{3}{L_0^4} \cdot 2\pi + O(\mu) < 0$ for the twist in RCP3BP.[*] It is possible for large L_0 that the $O(\mu)$-perturbation terms overwhelm the $-\frac{3}{L_0^4}$ and change the sign of twist term. This is why twisting can fail.

With an explicit twisting condition, a computer can be programmed to look for sign changes in the twist term. For $J_0 = 1.8$ and $\mu = 0.001$, numerics indicate a sign change somewhere after $16 \le L_{\text{twist}}^+(0.001, 1.8)$; that is, for eccentricities larger than 0.994 the map $\mathcal{F}_\mu$ may no longer be a twist map.

---

[*]Calculation of the twist term indicates that this sign should be positive; however, one must account for the fact that under the time rescaling in the energy reduction $\tilde{t} = g \approx -t$.

LEMMA 6.1

In Delaunay variables for RCP3BP$(0.001, 1.8)$, the map $\mathcal{F}_\mu$ is twisting for $e_{\text{twist}}^-(0.001, 1.8) \leq 0.07 \leq e \leq 0.994 \leq e_{\text{twist}}^+(0.001, 1.8)$.

Proof

A computer can be programmed to compute the partial derivative symbolically, then evaluate the twist term and verify that it remains of constant sign for $L \in [1.611, 15.94]$. Converting this into a statement about eccentricity gives the claimed bounds.   □

Remark. In [GK1], we establish a coordinate system that is twisting for nearly parabolic motions and does not require this lemma.

7. The applicability of Aubry-Mather theory to the RCP3BP

In Section 6, we showed that the map $\mathcal{F}_\mu$ is an EAPT on a certain domain, and hence it is possible to apply the results of Aubry-Mather theory where the map is twisting. Recall that the map $\mathcal{F}_\mu$ is defined as follows. We start with the RCP3BP in Delaunay coordinates. Then we reduce to the 3-dimensional energy surface $\mathcal{S}(J_0)$. The restricted dynamics has a naturally defined Poincaré map $\mathcal{F}_\mu : \{g = 0\} \rightarrow \{g = 0\}$. However, the action comparison was formulated in polar coordinates, and the comparison was performed with the Lagrangian dual to the polar Hamiltonian which has 2 degrees of freedom. Not only have coordinate systems changed, but the dimension has been reduced.

Unfortunately and somewhat surprisingly, the Hamiltonian of RCP3BP in polar is convex, while in Delaunay coordinates it has a concave component (in L) and a degeneracy (in G). Thus, to connect polar and Delaunay dynamics requires additional care. In this section, we justify the connection between the polar Lagrangian and the map $\mathcal{F}_\mu$. What we are really after is the following lemma.

LEMMA 7.1

Suppose that $\mathcal{F}_\mu$ has a rotational curve* $\mathcal{T}^1 \subset \text{Tw}^{\text{Del}}$. Then there is an action-minimizing rotational 2-torus $\mathcal{T}^2$ for the flow of the Hamiltonian H_{Polar}.

The plan is the following. We offer a proof of Lemma 7.1 which connects the dynamics of three dynamical systems, namely, the systems with H_{Polar}, H_{Del}, and $\mathcal{F}_\mu$. The lemma allows us to apply the action comparison method in polar coordinates to rule out the existence of rotational curves for the map $\mathcal{F}_\mu$. (Recall that rotational curves are obstructions to diffusion.) Next we work a bit to apply the so-called Mather connecting theorem to the map $\mathcal{F}_\mu$ in the region of instability. Special care must be taken since the

---

*Rotational curves are invariant curves which are not homotopically equivalent to single points.

instability region is not invariant. The Mather connecting theorem provides diffusing orbits for the map $\mathcal{F}_\mu$, and instabilities for the map $\mathcal{F}_\mu$ are mirrored by motions of the comet in polar coordinates.

Remark. In [GK1], we show that Delaunay variables are not well defined for nearly parabolic motions. Another coordinate system equipped with a symplectic change of coordinates $\mathcal{D}_{\mathrm{dyn}}$ allows us to formulate $\mathcal{F}_{\mathrm{dyn}}$, an EAPT for nearly parabolic motions. The machinery developed can then be applied to the EAPT $\mathcal{F}_{\mathrm{dyn}}$ to rule out invariant curves.

7.1. Proof of Lemma 7.1

$$\boxed{\text{1: Rotating Polar Coordinates: } H = H_{\mathrm{Polar}}(r, \varphi, P_r, P_\varphi)}$$

$$\Uparrow$$

$$\boxed{\text{2: Delaunay Coordinates: } H = H_{\mathrm{Del}}(\ell, L, g, G)}$$

$$\Updownarrow$$

$$\boxed{\text{3: Reduced Energy Coordinates: } \mathcal{F} = \mathcal{F}_\mu(\ell, L)}$$

First let us formulate the three systems described in the diagram above. Equation (2) formulates the RCP3BP in rotating polar coordinates with a Hamiltonian H_{Polar}. Given H_{Polar}, the Delaunay map $\mathcal{D}$ from Section 5 can be applied to convert from polar to Delaunay variables away from parabolic motions. The Hamiltonian becomes H_{Del} given by (9). It is not necessarily clear that H_{Del} is convex or that action minimizers exist. Consider the energy reduction procedure described in Appendix E.2 applied to the Hamiltonian H_{Del}. Call the energy-reduced Hamiltonian $\tilde{H}_{J_0}$. By construction, orbits of $\tilde{H}_{J_0}$ and orbits of H_{Del} are equivalent on the energy surface $\mathcal{S}(J_0)$ when G is written implicitly in terms of energy and the other Delaunay variables. $\tilde{H}_{J_0}$ is the time-periodic Hamiltonian with 1.5 degrees of freedom used in Section 6, and by the results of that section, the Poincaré map $\mathcal{F}_\mu$ formulated from $\tilde{H}_{J_0}$ is an EAPT on a certain domain.

LEMMA 7.2
There are no rotational curves for the map $\mathcal{F}_\mu$ if and only if there are no rotational 2-tori for the flow of the Hamiltonian H_{Del}.

Proof
This claim follows from the general results on Poincaré maps.   □

From the claim it suffices to show that a rotational 2-torus for the flow of the Hamiltonian H_{Del} maps under $\mathcal{D}$ to an action-minimizing rotational 2-torus for the flow of the Hamiltonian H_{Polar}. By action-minimizing, we mean action minimizing with respect to the Lagrangian L, which is the Legendre transform of the polar Hamiltonian H_{Polar}. To go between 1 and 2, some additional machinery is required. A priori when making a canonical change of coordinates, the image $\mathcal{D}(\mathcal{T}^2)$ of a rotational 2-torus $\mathcal{T}^2$ in Delaunay is not necessarily a graph over the base anymore. All that we can say is that $\mathcal{D}(\mathcal{T}^2)$ is an invariant object under the flow since the change of variables $\mathcal{D}$ is a smooth diffeomorphism away from parabolic motions.[*] Hence we must show that $\mathcal{D}(\mathcal{T}^2)$ is rotational and that it is action minimizing.

LEMMA 7.3
Suppose $\mathcal{T}^2$ is a rotational 2-torus for the flow of the Hamiltonian H_{Del}. Then $\mathcal{D}(\mathcal{T}^2)$ is a rotational 2-torus for the flow of the Hamiltonian H_{Polar}.

Proof
Suppose $\mathcal{T}^2$ is a rotational 2-torus for the flow of the Hamiltonian H_{Del}, and $\mathcal{D}(\mathcal{T}^2)$ is its image. We must show that the P_r and P_φ components of $\mathcal{D}(\mathcal{T}^2)$ are graphs over the base (r, φ). Since dynamics is restricted to the energy surface $H = -J_0$ in both coordinate systems, then it holds that

$$P_\varphi = P_\varphi(r, \varphi, P_r; J_0) = r^2 - \sqrt{r^4 + 2r - r^2\left(P_r^2 + 2J_0 + 2\Delta H(r, \varphi)\right)}.$$

Hence if we can show that P_r is a graph over the base, that is, $P_r = P_r(r, \varphi)$, then it follows that P_φ is also a graph over the base.

A careful analysis of the map $\mathcal{D}$ tells us

$$r = L^2\left(1 - e\cos(u)\right) \qquad Pr = \frac{Le\sin(u)}{r}$$

$$\varphi = g + 2\arctan\left(\sqrt{\frac{1+e}{1-e}}\tan\left(\frac{u}{2}\right)\right) \qquad P_\varphi = G$$

$$\ell = u - e\sin(u) \qquad e = \sqrt{1 - \frac{G^2}{L^2}}.$$

[*]We are bounded away from singularities in the mapping since $e \leq e_{\max} < 1$. In [GK1] a different coordinate change is considered to avoid singularities at $e = 1$.
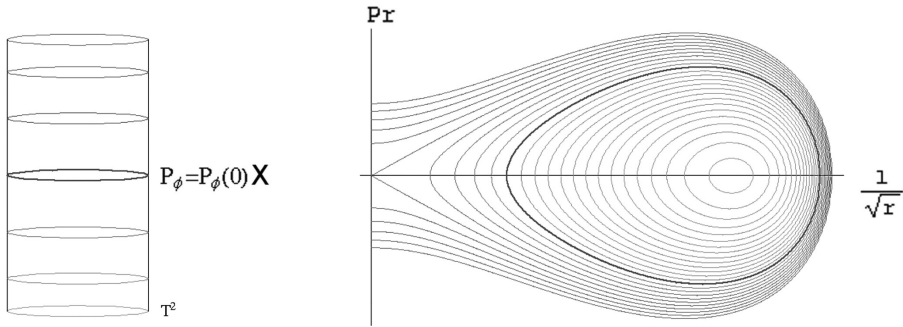
Figure 12. Integrable torus

For constant L and G (e.g., in the 2BP(SC)), then (r, P_r) is a function of the variable u only. It turns out that P_r is a double graph over r in an *onion* (see Figure 12). This is because fixing r fixes u, which in turn fixes P_r up to sign. Rotation inside the onion corresponds to rotation in the ℓ-direction; the *layer* of the onion corresponds to the L-direction. The G- and P_φ-directions are the same, and rotation in the g direction corresponds to rotation in the φ-direction. In this case, being rotational in Delaunay translates to being rotational in polar, with the caveat that the P_r may be a double graph.

The case when L, G are nonconstant is not that much worse. We seek to show the double-graph property for P_r; that is, we seek to show that $\mathcal{D}(\mathcal{T}^2) \cap \{P_r \geq 0\}$ and $\mathcal{D}(\mathcal{T}^2) \cap \{P_r \leq 0\}$ are graphs. Suppose not. Then there two points on $\mathcal{D}(\mathcal{T}^2)$ which have the same (r, φ)-coordinates but have two different P_r-coordinates, $P_r^1 > P_r^2 > 0$. But when $\dot{r} = P_r > 0$, then r is a monotone strictly increasing function. Furthermore, $\dot{\varphi} < 0$, so φ is a monotone strictly decreasing. Since $\mathcal{D}(\mathcal{T}^2)$ is invariant under the flow, there cannot be two distinct points (r, φ, P_r^1) and (r, φ, P_r^2) with $P_r^1 \neq P_r^2$ since this would contradict the monotonicity of r or φ. Hence the image of $\mathcal{D}(\mathcal{T}^2)$ is rotational. $\square$

The reason we desire the rotational (graph) property is the following lemma.

LEMMA 7.4 (McDuff and Salamon [MS, Lemma 9.6])
Suppose that $H : \Omega \times \mathbb{R}^n \to \mathbb{R}$, where $\Omega \subset \mathbb{R}^n$ is a Hamiltonian which satisfies the Legendre condition $\frac{\partial^2 H}{\partial p^2} > 0$. Moreover, assume that for every $q \in \Omega$ the map $\mathbb{R}^n \to \mathbb{R}^n$ given by $p \mapsto \partial_p H(q, p)$ has a global inverse so the inverse Legendre transformation gives rise to a Lagrangian $L : \Omega \times \mathbb{R}^n \to \mathbb{R}$. Let $S : \Omega \to \mathbb{R}$ be a solution of the Hamilton-Jacobi equation $H(q, \partial_q S) = E$. Suppose that $\gamma : [t_0, t_1] \to \Omega$ is invariant under the flow of H with $\dot{\gamma} = \partial_p H(q, \partial_q S(p))$, and suppose that $\xi : [t_0, t_1] \to \Omega$ is any absolutely continuous function such that $\xi(t_0) = \gamma(t_0)$

and $\xi(t_1) = \gamma(t_1)$. Then γ is action minimizing. Specifically,

$$\int_{t_0}^{t_1} L(\gamma, \dot{\gamma}) \, dt \le \int_{t_0}^{t_1} L(\xi, \dot{\xi}) \, dt.$$

To complete the proof of Lemma 7.1, we appeal to Lemma 3.1, which states that rotational 2-tori in polar are action minimizers. This turns out to be a corollary of Lemma 7.4.

Proof of Lemma 3.1
The polar Hamiltonian for RCP3BP satisfies the requirements of Lemma 7.4; namely, it is convex (see Lemma E.1). However, one must be a bit careful in its application. Lemma 7.4 requires that if an invariant curve γ is contained inside of an invariant torus $\mathcal{T}^2$, then $\mathcal{T}^2$ is a graph over the base. In polar, we must have that $P_r = P_r(r, \varphi)$ and $P_\varphi = P_\varphi(r, \varphi)$ are graphs over (r, φ) on the invariant torus. In Lemma 7.3 we argued that in fact there is a small ambiguity arising from the fact that $\pm P_r(r, \varphi)$ could both be on an invariant torus (e.g., an invariant curve could pass through an apohelion or perihelion which causes the sign of P_r to change). It is true that $\mathcal{T}^2 \cap \{P_r \ge 0\}$ and $\mathcal{T}^2 \cap \{P_r \le 0\}$ are graphs over (r, φ). To apply Lemma 7.4 for an invariant curve γ, note that it suffices to decompose γ into pieces, where $P_r \ge 0$ and $P_r \le 0$, and apply Lemma 7.4 to the respective pieces.

   This completes the proof of Lemma 7.1.   □

7.2. Connecting orbits
If C_- and C_+ are two rotationally invariant curves such that there are no invariant curves in between C_- and C_+, we say that the invariant region C bounded by C_- and C_+ is an *RI*. In invariant RIs, Birkhoff showed the existence of orbits coming arbitrarily close to C_- and C_+ (see [MF]). We need a similar but stronger result given by Mather [M1], [M2].

THEOREM 7.5 (Mather connecting theorem)
Suppose that $\omega_1 < \alpha_1, \alpha_2 < \omega_2$, and suppose that there are no rotationally invariant curves with rotation number $\omega \in (\omega_1, \omega_2)$ in an invariant (Birkhoff) rotationally invariant. Then there is a trajectory in the phase space whose α-limit set lies in the Aubry-Mather set Σ_{α_1} and whose ω-limit sets lies in Σ_{α_2}. Moreover, for a sequence of rotation numbers $\{\alpha_i\}_{i \in \mathbb{Z}}$, $\alpha_i \in (\omega_1, \omega_2)$, and a sequence of positive numbers $\{\epsilon_i\}$, there exists an orbit in the phase space $\{p_j\}$ and an increasing biinfinite sequence of integers $j(i)$ such that the $\mathrm{dist}(\Sigma_{\alpha_i}, p_{j(i)}) < \epsilon_i$ for all $i \in \mathbb{Z}$.

The semiinfinite region we consider is not necessarily invariant due to the fact that Delaunay variables are not defined for nearly parabolic motions. Furthermore, the

region Tw^{Del} where $\mathcal{F}_\mu$ is twisting is *not* invariant; however, it *is* free of invariant curves. Hence, Theorem 7.5 does not directly apply.

Let $\omega_{\min} = \inf\{\omega : \Sigma_\omega \subset Tw^{\text{Del}}\}$, and let $\omega_{\max} = \sup\{\omega : \Sigma_\omega \subset \text{Tw}^{\text{Del}}\}$ be the minimal and maximal rotation numbers for Aubry-Mather sets which are contained in the twist region, respectively.

LEMMA 7.6
There is a continuous function $\alpha_\omega > 0$ such that for all $\omega \in [\omega_{\min}, \omega_{\max}]$, there is an α_ω–neighborhood of Σ_ω contained in Tw^{Del}.

Proof
This follows from results for localization of Aubry-Mather sets found in [GK2]. We offer a coarse version of localization now.

Recall that estimates on change in angular momentum tell us that making one full revolution about the Sun does not change angular momentum by more than 8.95μ (see Lemma 4.2). Translating this into a statement about eccentricity, it says that starting with initial eccentricity $e_0 \leq e_{\max} = 0.96$, the comet remains in the twist region Tw^{Del} after one revolution around the Sun. Hence, starting in $\{e \leq 0.96 < e^+_{\text{twist}} = 0.994\}$ ensures that our Aubry-Mather sets remain bounded safely inside the twist region.   □

Let us consider the collection of all α_ω-neighborhoods

$$\alpha(\omega_{\min}, \omega_{\max}) := \bigcup_{\omega \in (\omega_{\min}, \omega_{\max})} \alpha_\omega(\Sigma_\omega).$$

Claim
The connecting orbits found in the Mather connecting theorem belong to $\alpha(\omega_{\min}, \omega_{\max})$.
The claim follows from careful study of Mather's original proofs. Xia [X1] contains a simpler approach to these results. The basic idea is that *almost-connecting* orbits remain in a neighborhood of Aubry-Mather sets. We now focus on applying Mather's connecting theorem.

It is known that every rotation number $\omega \geq 0$ has a nonempty Aubry-Mather set associated to it. Furthermore, it is known that Aubry-Mather sets are ordered by rotation number ω with Σ_ω and $\Sigma_{\omega'}$ close in the sense of Hausdorff distance for ω and ω' close (see [B], [MF]). Smaller rotation numbers correspond to slower rotation around the base $\mathbb{T}$ in the ℓ-direction. But this is to say that smaller rotation numbers correspond to higher eccentricities.

To get a diffusing orbit in polar coordinates, we use the Mather connecting theorem to provide the existence of an orbit of $\mathcal{F}_\mu$ with the desired properties. Specifically,
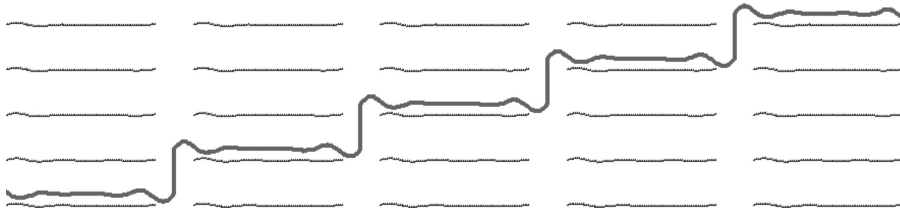
Figure 13. A diffusing orbit (ℓ vs. e)

let us choose the rotation numbers corresponding to eccentricities near $e = e^*(\mu, J_0)$ and $e = e_{\max}(\mu, J_0)$ and pick the $\{\epsilon_i\}$ to come arbitrarily close to the desired rotation numbers.

One could visualize the Aubry-Mather sets as the remainders of tori after a perturbation has filled them with infinitely many small holes. To envision a diffusing orbit, first imagine unrolling the cylinder on the real plane. A diffusing orbit is one which "climbs a set of stairs," that is, increases in the holes of the Aubry-Mather set and then follows the remnants of a torus of higher rotation number for a while. The largest increase ("taking a step") occurs primarily at times when the comet is at the perihelion.

In the sequel [GK1], we use the Mather connecting theorem, to construct oscillatory orbits, and Chazy motions (see [AKN] for a discussion of Chazy motions). Mathematically this corresponds to picking a more complicated sequence of Aubry-Mather sets for the connecting orbit to visit.

8. Conclusion and extension

What prevents us from extending the result to eccentricities beyond $e_{\max}$ is the fact that our coordinate system becomes undefined for nearly parabolic motions. This is not an ideological issue, as we expect instabilities near the separatrices which arise from parabolic motions. Delaunay variables can be modified near the separatrices to deal with singularities which arise for nearly parabolic motions, and this is done in [GK1]. When done, our claim becomes the following.

THEOREM 8.1
Consider the RCP3BP(μ, J_0) with dynamics restricted to $\mathcal{S}^{\mathrm{out}}(J_0)$. There exists a function $e^*(\mu, J_0)$, and there exist trajectories of a comet with initial eccentricity $e_0 > e^*(\mu, J_0)$ that increase in eccentricity beyond one in a manner such that the comet escapes the solar system to infinity. For example, if $\mu = 10^{-3}$ and $J_0 = 1.8$, then $e^* \leq 0.66$.

The methods of Section 7 can be applied to show the following.

COROLLARY 8.2

Under the hypothesis of Theorem 8.1, all possible Chazy motions are realized.

Appendices

A. Rigorous numerics

"Let anyone integrate them who can."
Clairaut

We need a computer to provide mathematically verified bounds on flows of ODEs to complete some of the estimates encountered in Theorem 4.4 as well as results in [GK1] and [GK2]. Consider the initial value problem (IVP)

$$\begin{cases} \dot{x} = f(x), \\ x(0) = x_0. \end{cases} \tag{11}$$

Assume that solutions exist, are unique, and are defined for all time and that f is sufficiently smooth (either C^∞ or real analytic). We specify a fixed step size h in time. If $x(t)$ is a solution to the IVP, then from Taylor's theorem

$$x(t + h) = x(t) + hx'(t) + O(h^2) \approx x(t) + hf\big(x(t)\big),$$

Euler's method forgets the remainder and makes a linear approximation at each time step to give

$$\begin{cases} t_i = t_{i-1} + h, \\ x_i = x_{i-1} + hf(x_{i-1}). \end{cases}$$

Each step of the Euler method (which is an example of a first-order Taylor method) makes an error of $O(h^2)$. Errors made truncating Taylor series methods are known as the *local truncation errors*, which for h small are usually not too bad. However, the small errors made by disregarding the $O(h^2)$-term causes the method to track a slightly different solution after each time step. After many steps these small errors can accumulate and destroy the method's usefulness by tracking to a solution which has different behavior from the one desired. This is known as *global truncation error*. Even higher-order Taylor methods as well as Runge-Kutta methods are still susceptible to this. We utilize methods which avoid these difficulties.

A.1. Interval arithmetic

When working on a computer, there is another source of error which must be accounted for—floating point error—which arises because a computer is incapable of representing most real numbers.

  Machine representable numbers are a subset of real numbers with which a computer can perform computations. We define *machine-ϵ* as the smallest positive number such that $1 \neq (1+\epsilon)$ on our machine. It gives a kind of spacing between machine representable numbers. This is dependent on the computer's architecture and software;

however, most computers adopt the Institute of Electronical and Electronics Engineers (IEEE) standards which specify such representable numbers, and use machine $\epsilon \approx 10^{-16}$. Assume that we have adopted a standard such as [IEEE].

One method to get around the difficulties of machine representability is by using so-called *interval arithmetic*. If $x \in \mathbb{R}$ we say that $[a, b]$ is an *interval representation* for x with machine representable numbers a and b if $x \in [a, b]$. We denote intervals in calligraphic capital letters, for example, $\mathcal{I}$. If $\mathcal{I} = [a, b]$, then define $\max(\mathcal{I}) = b$ and $\min(\mathcal{I}) = a$.

If $f : \mathbb{R}^n \times \mathbb{R}^m \to \mathbb{R}$ is a smooth function and $\mathcal{I} \times \mathcal{J}$ is a product of intervals, we say that the interval $\mathcal{K}$ *encloses* f on the domain $\mathcal{I} \times \mathcal{J}$ if $f(\mathcal{I}, \mathcal{J}) \subset \mathcal{K}$. Computing good enclosures is a principal difficulty in interval arithmetic. References [KM] and [MZ] contain methods to make enclosures both rigorous and efficient. For a different approach, see [BM].

When we say "bound $f : \mathbb{R}^d \to \mathbb{R}$ over the domain D using interval arithmetic" we really mean to use the following algorithm:

(1)   cover D with n intervals (or products of intervals) $\mathcal{I}_i^d$ so that $D \subset \bigcup_i^n \mathcal{I}_i^d$;

(2)   find enclosures $\mathcal{K}_i$ such that $f(\mathcal{I}_i^d) \subset \mathcal{K}_i$;

(3)   compute $m = \min(\mathcal{K}_i)$ and $M = \max(\mathcal{K}_i)$.

This algorithm generates numbers so that $f(x) \in [m, M]$ for all $x \in D$. The bounds depend on D, d, n, and the regularity of f. Generally speaking, decreasing $\operatorname{diam}(\mathcal{I}_i^d)$ improves the bounds.

Several of our computations are done on a computer algebra system (CAS). For our purposes, a *CAS* is a program which rigorously manipulates algebraic and numerical expressions. A CAS can be programmed to use *exact arithmetic*, which is arithmetic that uses symbolic expressions to produce exact output without rounding. For example, $1/2 + 1/3 = 5/6$ on a CAS. It is possible to perform *exact interval arithmetic* where intervals contain symbolic expressions and the bounds are manipulated using exact arithmetic. We require a CAS with the following capabilities. It must be able to

(1)   manipulates algebraic expressions using exact arithmetic;

(2)   take symbolic derivatives (where possible);

(3)   take symbolic integrals (where possible);

(4)   manipulate formal power series (where possible);

(5)   perform interval arithmetic accounting for rounding error.

As our estimates require many lower and upper bounds, let us adopt the notation $(\cdot)^{\pm}$ to denote functions or numbers which are upper and lower bounds on the function $(\cdot)$. For a function $f(x, y)$ defined on the domain $\mathcal{I} \times \mathcal{J}$, let "$f(x, y) \leq (f(x))^+$" mean that $(f(x))^+$ is a function of $x \in \mathcal{I}$ such that the bound holds for all $y \in \mathcal{J}$ in the domain of f. As such a function is not necessarily well defined, explicit constructions are given whenever this notation is used.

Returning to the problem of rigorous numerics for ODEs, let us reformulate the problem in terms of interval arithmetic. Now consider the *interval value problem* (IvVP)

$$\begin{cases} \dot{x} = f(x), \\ x(0) \in \mathcal{I} = [x_0 - w, x_0 + w], \end{cases} \tag{12}$$

where now $\mathcal{I}$ is some interval of initial conditions (a w-window around x_0), x is now a product of intervals in $\mathbb{R}^d$, and all operations are performed via interval arithmetic. From a dynamical systems perspective, we seek to transport a cube of initial conditions under the flow of the ODE. The advantage of an IvVP solver is that by covering the space of initial conditions with intervals, the solver tells us rigorously how the entire space moves under flow. This is because the flow of the IVP given in (11) is rigorously contained inside the flow of the IvVP given by (12).

A.1.1. CAPD

One might wonder how to construct a rigorous IvVP solver or even if they exist. Both questions are answered in [Z] and [WZ]. The main idea is as follows.

Recall that the difficulty with nonrigorous methods is that they follow slightly different solutions at each step. Gronwall's inequality tells us that differing solutions move apart at most exponentially based on the magnitude of a Lipschitz constant, which is roughly $||Df(x)||$. For example, the $O(h^2)$ local truncation error in Euler's method is from the remainder term in Taylor's theorem which can be written in the form $x''(\xi)h^2/2 = Df(\xi)f(\xi)h^2/2$ for some ξ. A naive way to produce a rigorous integrator is to bound the truncation error at each step. Poor bounds on the remainder require the integrator to use larger and larger interval bounds after each step, and these bounds can potentially grow exponentially, rendering the output useless. This is commonly known as the *wrapping effect*. It arises not only from Euler's method, but from higher-order methods as well.

To get tight estimates on the errors made after each step, accurate estimates of $||Df(x)||$ are needed. In [Z], [WZ], and [MZ], efficient methods are outlined to do this. They introduce efficient representations of interval sets that allow for better bounds and introduce an alternative to Gronwall's inequality which appropriately deals with exponential decay. It is also noted that when solving equations of variation, the same main idea can be applied to $D^2 f(x)$ and higher derivatives so that one can get efficient bounds for higher-order equations of variation. This is useful in the sequels to this paper (see [GK1], [GK2]).

The theory developed in [Z] and [WZ] has been implemented in a package called CAPD. It is our primary tool for rigorous integration of the equations of motion.

B. Estimates on perturbation terms

We need tight estimates on the perturbation term ΔH and its derviatives to get good numerics. The Taylor series expansion of ΔH in $1/r$ yields

$$\Delta H(r, \varphi; \mu) = \sum_{i=1}^{\infty} (-1)^i \frac{\mu(1-\mu)(\mu^i - (\mu-1)^i)}{r^{i+2}} P_{i+1}(\cos(\varphi)),$$

where P_i is the ith Legendre polynomial and is given by the recursive formula

$$(i+1)P_{i+1}(x) = (2i+1)x P_i(x) - i P_{i-1}(x)$$

(see formula (1)).

Expansions of Newtonian potentials were one of the reasons Legendre considered these polynomials. In fact,

$$\frac{1}{\sqrt{1 - 2xt + t^2}} = \sum_{n=0}^{\infty} P_n(x)t^n.$$

For $x \in (1, 1)$, $|P_i(x)| < 1$ and $|P_i(\pm 1)| = 1$. From this, one concludes that the series expansion for ΔH converges provided μ is small and $r > 1 + \mu$, for example, when the comet is in the outside region. One can also show that $|P_i'(x)| \leq (i(i+1))/2$ for $x \in [-1, 1]$. See, for example, [R] for formulas and derivation of Legendre polynomials.

Bounding the Legendre polynomials produce bounds on the perturbation terms which are independent of φ. Do this to define

$$(|\Delta H|)^+(r) := \frac{\mu(1-\mu)}{r(r+\mu-1)(r+\mu)},$$

$$\left(\left|\frac{\partial \Delta H}{\partial r}\right|\right)^+(r) := \frac{\mu(1-\mu)(\mu^2 + \mu(4r-1) + r(3r-2))}{r^2(r+\mu-1)^2(r+\mu)^2},$$

$$\left(\left|\frac{\partial \Delta H}{\partial \varphi}\right|\right)^+(r) := \frac{\mu(1-\mu)r(1 + 3r(r-1) + \mu(6r-3) + 3\mu^2)}{(r+\mu-1)^3(r+\mu)^3}.$$

Remark. All of these estimates are independent of the Jacobi constant and are $O(\mu/r^3)$ or better. They are used to produce bounds in Lemma 4.1.

B.1. Bounds on the perihelion

Consider the case $\mu = 10^{-3}$ and $J_0 = 1.8$. It is useful to have some initial bounds on angular momentum and minimal radius. The 2BP(SC) for elliptic and parabolic motions are known to have minimum perihelion radius $r^{\text{perih}} \geq J_0^2/2$.

One can easily prove for a fixed angle φ that the radius of the perihelion is decreasing as a function of P_φ. It suffices to examine perihelions at the φ-critical points of ΔH. The critical points are at $\varphi = 0, \pi$ and $\cos(\varphi) = (1 - 2\mu)/(2r)$. Since ΔH is algebraic in r at those critical points, a CAS can solve and find the minimum perihelion radius for elliptic and parabolic motions. This is how Lemma 1.1 is proved. Doing so for $J_0 = 1.8$ and $\mu = 10^{-3}$ yields the $r^{\mathrm{perih}} \geq 1.61839 \geq (1.8^2)/(2) - 8\mu$.

The class of solutions we analyze has $P_\varphi \leq 1.81$; that is, $e \leq 1.0324$. Computing the minimum perihelion radius for this class yields

$$r^{\mathrm{perih}} \geq 1.61048 = r^{\mathrm{perih}}_{\min} \qquad |\Delta H| \leq 0.629509\mu.$$

B.2. Estimation of $\dot{g}$

LEMMA B.1

Fix $\mu = 10^{-3}$ and $J_0 = 1.8$. Then $\left|\frac{\partial \Delta H}{\partial G}\right| \leq 0.025$, and hence $\dot{g} = -1 + \frac{\partial \Delta H}{\partial G} < 0$.

Proof

Let us begin by computing

$$\frac{\partial \Delta H}{\partial G} = \frac{\partial \Delta H}{\partial r}\frac{\partial r}{\partial G} + \frac{\partial \Delta H}{\partial \varphi}\frac{\partial \varphi}{\partial G}.$$

It is possible to bound $\left|\frac{\partial \Delta H}{\partial r}\right|$ and $\left|\frac{\partial \Delta H}{\partial \varphi}\right|$ with $\left(\left|\frac{\partial \Delta H}{\partial r}\right|\right)^+$ and $\left(\left|\frac{\partial \Delta H}{\partial \varphi}\right|\right)^+$, respectively. Using $r \geq r^{\mathrm{perih}}_{\min} = 1.61048$, one finds $\left|\frac{\partial \Delta H}{\partial r}\right| \leq 1.81101\mu$ and $\left|\frac{\partial \Delta H}{\partial \varphi}\right| \leq 6.65233\mu$.

One can compute (via a CAS)

$$\frac{\partial r}{\partial G} = \frac{G(G^2 - r)}{re^2}, \qquad \frac{\partial \varphi}{\partial G} = \frac{L(G + r)\sin(u)}{r^2 e};$$

$\frac{\partial r}{\partial G}$ has critical points at $u = 0, \pi$ (recall $r = L^2(1 - e\cos(u))$). Evaluation at the critical points gives the bound $\left|\frac{\partial r}{\partial G}\right| \leq \frac{G}{e}$. Using $e \in [0.5, 1.1]$ and $G \in [1.6, 1.82]$ gives us $\left|\frac{\partial r}{\partial G}\right| \in [1.45455, 3.64]$.

The story for $\frac{\partial \varphi}{\partial G}$ is a bit more complicated. One can compute the critical points in u and find two critical points u_1 and u_2 (these are found with a computer algebra system). The critical point u_2 is a complex root for $e < 1$, and for $e > 1$, $\frac{\partial \varphi}{\partial G}\big|_{u=u_2}$ is complex. Hence u_2 can be disregarded. It turns out that $\frac{\partial \varphi}{\partial G}\big|_{u=u_1} = \frac{f(e)}{G}$, where $f(e)$ is a function of e only. For $e \in [0.5, 1.1]$, then $f(e) \in [2.03336, 4.11667]$. Using $G \in [1.6, 1.82]$ yields $\left|\frac{\partial \varphi}{\partial G}\right| \in [1.11723, 2.57292]$.

Hence $\left|\frac{\partial \Delta H}{\partial G}\right| \leq 1.81101\mu \cdot 3.64 + 6.65233\mu \cdot 2.57292 = 0.023708 < 0.025.$ □

C. Estimates on change in angular momentum

In this appendix, we prove Lemma 4.2 on the change in angular momentum. Recall that

$$\dot{P}_\varphi = -\frac{\partial \Delta H}{\partial \varphi}.$$

Hence

$$\Delta P_\varphi(t_0, t_1) = P_\varphi(t_1) - P_\varphi(t_0) = \int_{t_0}^{t_1} -\frac{\partial \Delta H}{\partial \varphi} \, dt.$$

Now

$$\frac{d}{dt}\big(\Delta H(r(t), \varphi(t))\big) = \Big(\frac{\partial \Delta H}{\partial r}(t)\Big)\dot{r}(t) + \Big(\frac{\partial \Delta H}{\partial \varphi}(t)\Big)\dot{\varphi}(t),$$

and hence

$$\frac{\partial \Delta H}{\partial \varphi}(t) = \frac{1}{\dot{\varphi}(t)}\Big(\frac{\partial \Delta H}{\partial r}(t)\dot{r}(t) - \frac{d}{dt}(\Delta H(t))\Big).$$

Plugging in and using a change of variables gives

$$\Delta P_\varphi(t_0, t_1) = \int_{t_0}^{t_1} -\frac{1}{\dot{\varphi}(t)}\Big(\frac{\partial \Delta H}{\partial r}(t)\dot{r}(t) - \frac{d}{dt}\Delta H(t)\Big) \, dt$$

$$= \int_{t_0}^{t_1} \frac{1}{\dot{\varphi}(t)}\Big(\frac{d}{dt}\Delta H(t)\Big) \, dt - \int_{r(t_0)}^{r(t_1)} \frac{1}{\dot{\varphi}(t(r))}\Big(\frac{\partial \Delta H}{\partial r}\Big)\big(r, \varphi(t(r))\big) \, dr.$$

Let $r_0 = r(t_0)$ and $r_1 = r(t_1)$. Suppose that the comet is approaching the perihelion from the preceding aphelion or from infinity. Then $r_1 \leq r_0$. As t increases, r decreases, and our estimate should account for more uncertainty in the value of P_φ given that the perturbation term grows larger in magnitude closer to the Sun:

$$|\Delta P_\varphi(t_0, t_1)| \leq \frac{1}{\min_{r \in [r_0, r_1]} |\dot{\varphi}(r)|}\Big(\Big|\int_{t_0}^{t_1} \frac{d}{dt}\Delta H(t) \, dt\Big| + \int_{r_1}^{r_0} \Big|\frac{\partial \Delta H}{\partial r}\Big| \, dr\Big).$$

Note that

$$\min_{r \in [r_0, r_1]} |\dot{\varphi}(r)| \geq \min_{r \in [r_0, r_1]} \Big(1 - \frac{P_\varphi}{r^2}\Big) \geq 1 - \frac{\max P_\varphi}{r_1^2}.$$

Hence

$$|\Delta P_\varphi(t_0, t_1)| \leq \frac{1}{1 - \frac{\max P_\varphi}{r_1^2}}\Big(|\Delta H(t_1) - \Delta H(t_0)| + \int_{r_1}^{r_0} \Big|\frac{\partial \Delta H}{\partial r}\Big| \, dr\Big).$$

$$\leq \frac{1}{1 - \frac{\max P_\varphi}{r_1^2}}\Big((|\Delta H|)^+(r_0) + (|\Delta H|)^+(r_1) + \int_{r_1}^{r_0} \Big(\Big|\frac{\partial \Delta H}{\partial r}\Big|\Big)^+ dr\Big).$$

Claim
Note that $\left((|\Delta H|)^+(r_0) + (|\Delta H|)^+(r_1) + \int_{r_1}^{r_0} \left(\left|\frac{\partial \Delta H}{\partial r}\right|\right)^+ dr\right)$ is nondecreasing as a function of r_0 for $r_0 \geq r_1 \geq 1 + \mu$.

Proof
Differentiate with respect to r_0, and note the derivative is identically zero.   □

Since $(|\Delta H|)^+$ is decreasing as a function of r and $\lim_{r_0 \to \infty}(|\Delta H|)^+(r_0) = 0$, from this claim it follows that

$$|\Delta P_\varphi(t_0, t_1)| \leq \rho\big(r(t_1)\big) = \rho(r_1)$$

$$:= \frac{1}{1 - \frac{\max P_\varphi}{r_1^2}} \left((|\Delta H|)^+(r_1) + \int_{r_1}^{\infty} \left(\left|\frac{\partial \Delta H}{\partial r}\right|\right)^+ dr\right),$$

provided that the radius is decreasing from t_0 to t_1. Using $(\max P_\varphi) = 1.81$ to evaluate $\rho(5)$ gives an upper bound on the change of P_φ over the whole outside region. Note that this argument can be made symmetric by considering change from the final conditions and reversing time. Hence, when approaching the perihelion from the preceding apohelion or from infinity,

(1)   angular momentum does not change by more than $\rho(5) \approx 0.0215298\mu$ over the entire outside region,

(2)   angular momentum does not change by more than $\rho(r_{\min}^{\mathrm{perih}}) \approx 4.44885\mu$, and

(3)   angular momentum does not change by more than $2\rho(5) + 2\rho(r_{\min}^{\mathrm{perih}}) \approx 8.94077\mu$ during an R-solar passage.

Note that the construction allows for any type of R-solar passage, elliptic, parabolic, or hyperbolic, provided that $P_\varphi \leq 1.81$ during the passage.

   If we only care about change in angular momentum after an R-solar passage, then (3) is not an optimal bound. We use CAPD to perform rigorous integration over all 5-solar passages with $P_\varphi \in [1.68753, 1.81]$ and note that $|\Delta P_\varphi| \leq 1.4\mu$ (see Theorem 4.4). Thus a more tight estimate on total change in angular momentum after an R-solar passage is $1.4\mu + 2 \cdot 0.0215298\mu < 1.444\mu$.

   This justifies the initial choice of $P_\varphi \leq 1.81$ in the analysis, since if the comet starts with $P_\varphi(0) = 1.8$ (i.e., $e = 1$) and approaches the Sun to make an R-solar passage, then the most angular momentum could ever be is $P_\varphi = 1.80894077 < 1.81$. Comets with angular momentum slightly above $P_\varphi = J_0$, that is, slightly above $e = 1$ after a 5-solar passage, escape the solar system. Note that $e \leq 0.96$ corresponds to $P_\varphi \leq 1.788$, so after an R-solar passage, escape is not possible.

Remark. We have implicitly used $J_0 = 1.8$ and $\mu = 10^{-3}$ to generate the estimate on change in angular momentum since these constants are used in estimates on ρ, $(|\Delta H|)^+$, and $\left(\left|\frac{\partial \Delta H}{\partial r}\right|\right)^+$. The dependency on J_0 is not so strong; it was only used to

describe the domain of nearly parabolic motions, namely, to give $(\max P_\varphi) \leq 1.81$. The software to estimate this quantity can be adapted to other μ and J_0.

D. Table of integrals

Let us investigate some properties of the following commonly occurring integrals. At various times one encounters integrals of the form

$$\int_{t_0}^{t_1} r^k(t)\,dt = \int_{r_0}^{r_1} \frac{r^k}{\dot{r}}\,dr.$$

Away from $e = 1$, this can be rewritten

$$F(J_0, r_0, r_1, P_\varphi, k) = \int_{r_0}^{r_1} \frac{r^{k+1}dr}{\sqrt{2(J_0 - P_\varphi + \Delta H)(r_+ - r)(r - r_-)}}.$$

Suppose that it is possible to bound $(J_0 - P_\varphi + \Delta H)$ as well as $r_\pm$ independently of time, where $r_\pm$ are the apohelion and perihelion radii as given in (7). Then to evaluate the integral (D) it suffices to know how to evaluate

$$I(a, b, c, d, k) := \int_c^d \frac{r^k dr}{\sqrt{(b - r)(r - a)}},$$

where in all cases, $a, b, c, d \geq 0$ and $a \leq c \leq r \leq d \leq b$. Specific forms are known for some k:

$$I(a, b, c, d, -1) := \left(\frac{\arctan((x(a + b) - 2ab)/(2\sqrt{ab(b - x)(x - a)}))}{\sqrt{ab}} \right)\Big|_{x=c}^{x=d},$$

$$I(a, b, c, d, 0) := \left(\arcsin\left(\frac{2x - b - a}{b - a} \right) \right)\Big|_{x=c}^{x=d},$$

$$I(a, b, c, d, 1) := \left(\frac{a + b}{2} \arcsin\left(\frac{2x - a - b}{b - a} \right) - \frac{b - a}{2}\sqrt{1 - \left(\frac{2x - a - b}{b - a} \right)^2} \right)\Big|_{x=c}^{x=d}.$$

D.1. Integrals for hyperbolic motions

Using elongated solar passages to model behavior of the comet is only effective provided the comet is sufficiently elliptic; that is, eccentricity is sufficiently far from one. In the case $e \approx 1$, R-solar passages are used as defined in Section 3. However, to perform the action comparison, rigorous justification of behavior in the outside region is still needed. The method of using extreme 2BPs as in Section 4 can be applied; however, when computing extreme 2BPs it is possible that one or more have hyperbolic behavior. In this case, (7) is no longer valid. The hyperbolic analogue is

$$\int_{r_0}^{r_1} \frac{r^k}{\dot{r}}dr\dot{r} = \int_{r_0}^{r_1} \frac{r^{k+1}}{\sqrt{((1 + \sqrt{1 - 2P_\varphi^2(J_0 - P_\varphi - \Delta H)} - 2(J_0 - P_\varphi - \Delta H)r))(r - r_-)}}dr.$$

This formula comes about by carefully rearranging (7) to remove the apohelion term.

Examination of the interval estimates in Section 4 indicates that if the appropriate formulas for time, action, and difference in angle are given, then the estimates in Section 4 still hold. Since the comet does not make an elongated Solar passage where it moves from $r = 5$ to an apohelion to back to $r = 5$, then the multiplier of 2 is not needed in the formulas for t_{out} and T_{out} nor in similar formulas. Everywhere there is a 2ρ, it may be replaced with a ρ. Everywhere is an integral bound $2B_{\text{out}}(i)$, or $2D$, replace it with a $B_{\text{out}}(i)$, or D, respectively. These places are indicated in the text of Section 4.

80-Solar passages are used to perform very high eccentricity action comparisons. Use $R_+^\pm = 80$ wherever it appears in Section 4. If an extreme 2BP is elliptic, then it suffices to use $B_{\text{out}}(i)$'s as defined in Section 4. Otherwise the b's and B's must be modified to account for hyperbolic 2BPs.

The following are the analogues of the integrals from above for hyperbolic motions:

$$I^{hyp}(a, b, e, c, d, -1) = \left(\frac{2 \arctan(\sqrt{b(x-a)}/\sqrt{a(ex+b)})}{\sqrt{ab}} \right)\Big|_{x=c}^{x=d},$$

$$I^{hyp}(a, b, e, c, d, 0) = \left(\frac{2 \log(e\sqrt{x-a} + \sqrt{e(b+ex)})}{\sqrt{e}} \right)\Big|_{x=c}^{x=d},$$

$$I^{hyp}(a, b, e, c, d, 1) = \left(\frac{\sqrt{(ex+b)(x-a)}}{e} + \frac{ae-b}{e^{3/2}} \right.$$
$$\left. \times \log\left(e\sqrt{x-a} + \sqrt{e(b+ex)}\right) \right)\Big|_{x=c}^{x=d}.$$

New b_{out}'s and B_{out}'s (for 80-solar passages) are defined by

$$b_{\text{out}}^\pm(k) = I^{hyp}(r_-^\pm, x_\pm, y_\pm, 80, k) - I^{hyp}(r_-^\pm, x_\pm, y_\pm, 5, k),$$

$$B_{\text{out}}^\pm(k) = I^{hyp}(R_-^\pm, X_\pm, Y_\pm, 80, k) - I^{hyp}(r_-^\pm, x_\pm, y_\pm, 5, k),$$

$$x_\pm = 1 + \sqrt{1 + 2(P_\varphi \pm \rho(5) \pm w)^2(P_\varphi \pm \rho(5) \pm w - J_0)},$$

$$X_\pm = 1 + \sqrt{1 + 2(P_\varphi \pm \rho(5) \pm w \pm M)^2(P_\varphi \pm \rho(5) \pm w \pm M - J_0)},$$

$$y_\pm = = 2(P_\varphi \pm \rho(5) \pm w - J_0),$$

$$Y_\pm = = 2(P_\varphi \pm \rho(5) \pm w \pm M - J_0),$$

where $w, M, r_-^\pm$, and $R_-^\pm$ are defined as in Section 4. Such bounds are easily computable on a computer.

E. Lemmas on convexity and energy reduction

In this appendix, we prove some of the lemmas used in Section 7 supporting the applicability of Aubry-Mather theory.

E.1. Polar convexity

LEMMA E.1

Let $H = H_{\mathrm{Polar}}$ be the Hamiltonian associated to RCP3BP given by (2). Then H and $\exp(H)$ are convex.

Proof

Explicit computation reveals for $q = (r, \varphi)$, $p = (P_r, P_\varphi)$ that

$$\mathrm{Det}(\partial_{pp} H) = \frac{1}{r^2} > 0,$$

$$\mathrm{Tr}(\partial_{pp} H) = 1 + \frac{1}{r^2} > 0.$$

Hence $\partial_{pp} H$ is positive definite, and the claim follows. □

E.2. Energy reduction

In this section, we outline a method to produce a time-periodic Hamiltonian with $(n - 1)$ degrees of freedom from an autonomous Hamiltonian with n degrees of freedom with trajectories restricted to an energy surface. This method can be found in [A] (see also [BK]).

Suppose that $H = H(I_1, \ldots, I_n, \theta_1, \ldots, \theta_n)$ is a Hamiltonian with solutions 2π-periodic in the $\theta_1, \ldots, \theta_n$ variables and suppose $\frac{\partial H}{\partial I_n} \neq 0$. Consider the Hamiltonian H' defined by

$$dH' = \sum_i^n \frac{\left(\frac{\partial H}{\partial I_i}\right)}{\left(\frac{\partial H}{\partial I_n}\right)} dI_i + \frac{\left(\frac{\partial H}{\partial \theta_i}\right)}{\left(\frac{\partial H}{\partial I_n}\right)} d\theta_i.$$

Then trajectories of H and H' are identical up to rescaling of time by $\tilde{t} = \theta_n(t)$. Fix an energy surface $H = E$. This implicitly fixes one of the variables, say, $I_n = I_n(I_1, \ldots, I_{n-1}, \theta_1, \ldots \theta_n)$. Consider the Hamiltonian

$$\tilde{H}(I_1, \ldots, I_{n-1}, \theta_1, \ldots \theta_n)$$
$$= H'\big(I_1, \ldots, I_{n-1}, \theta_1, \ldots \theta_n, I_n(I_1, \ldots, I_{n-1}, \theta_1, \ldots \theta_n)\big)$$
$$- I_n(I_1, \ldots, I_{n-1}, \theta_1, \ldots \theta_n).$$

Then $\frac{\partial \tilde{H}}{\partial I_n} = 0$ and for $i < n$, $\frac{\partial \tilde{H}}{\partial I_i} = \frac{\left(\frac{\partial H}{\partial I_i}\right)}{\left(\frac{\partial H}{\partial I_n}\right)}$. Hence $\tilde{H}$ does not depend on I_n. We think of $\tilde{H}$ as a time-periodic Hamiltonian with time $\tilde{t} = \theta_n$.

F. Appendix. Hardware and software

Mathematica was used for its symbolic manipulation abilities as well as its built-in interval arithmetic. It was used to verify the claims in the above technical appendices. It also is used to differentiate symbolically the perturbation term in Delaunay variables and compute the twist term. Furthermore, Mathematica's built-in numerical differential equation solver allowed us to model results quickly and get estimates on the quantities involved in the action comparison. We made heavy use of the CAPD library which is written in C++ to perform the rigorous numerical integration. CAPD* is a library which provides objects for intervals, vectors, matrices, maps, and integrators which can be included into C++ programs. The libraries were used to perform the action comparison rigorously.

The programs Mathematica and CAPD are packaged with a guide which gives explicit details on which programs carry out which parts of the proof, as well as information on obtaining libraries, compiling, running, and modifying the code for use on similar problems. Logs and outputs of some of the programs are also included due to the length of time needed to generate the data.

Most of the software ran continuously for 2 weeks, distributed over a cluster of 15 machines, the fastest of which was a 3.4-GHz Pentium 4 with 2 GB RAM and a 120-GB HDD. It produced over 16 GB of data. Each machine was running a variant of Linux with the latest available build of CAPD and Mathematica 5.0 or better.

---

*CAPD can be obtained at capd.ii.uj.edu.pl. The programs written in Mathematica and CAPD can be obtained online at www.math.umd.edu/˜joepi.

References

[A]   V. I. ARNOL'D, *Mathematical Methods of Classical Mechanics*, translated from the
         1974 Russian original by K. Vogtmann and A. Weinstein, 2nd ed., corrected
         reprint, Grad. Texts in Math. **60**, Springer, New York, 199?. MR 1345386

[AKN]   V. I. ARNOL'D, V. V. KOZLOV, and A. I. NEISHTADT, *Mathematical Aspects of
         Classical and Celestial Mechanics*, *Dynamical Systems. III*, translated from the
         Russian original by E. Khukhro, 3rd ed., Encyclopaedia Math. Sci. **3**, Springer,
         Berlin, 2006. MR 2269239

[Al]   V. M. ALEKSEYEV, *Sur l'allure finale du mouvement dans le probléme des trois corps*,
         Congrès Internat. Mathématiciens (Nice, 1970) **2**, Gauthier-Villars, Paris, 1971,
         893–907.

[B]   V. BANGERT, "*Mather sets for twist maps and geodesics on tori*", Dynamics Reported
         1, 1–56, Dynam. Report. Ser. Dynam. Systems Appl. **1**, Wiley, Chichester, 1988.
         MR 0945963

[BK]   J. BOURGAIN and V. KALOSHIN, *On diffusion in high-dimensional Hamiltonian
         systems*, J. Funct. Anal. **229** (2005), 1–61. MR 2180073

[BM]   M. BERZ and K. MAKINO, *Verified Global Optimization with Taylor Model-based
         Range Bounders*, Transact. Computers **4** (2005), November.

[BoMa]   S. BOLOTIN and R. S. MACKAY, *Nonplanar second species periodic and chaotic
         trajectories for the circular restricted three-body problem*, Celestial Mech.
         Dynam. Astronom. **94** (2006), 433–449. MR 2245344

[CC]   A. CELLETTI and L. CHIERCHIA, *KAM stability and celestial mechanics*, Mem. Amer.
         Math. Soc. **187** (2007), no. 878. MR 2307840

[CC1]   ———, Personal communication, 2006.

[F]   A. FATHI, *Weak KAM Theorem in Lagrangian Dynamics*, Tenth Preliminary Version.

[G]   C. GOLÉ, *Symplectic Twist Maps: Global Variational Techniques*, Adv. Series
         Nonlinear Dyn. **18**, World Sci., River Edge, N.J., 2001. MR 1992005

[GK1]   J. R. GALANTE and V. KALOSHIN, *Construction of a Twisting Coordinate System for
         the Restricted Circular Planar Three Body Problem*, preprint, available at
         http://www-users.math.umd.edu/˜joepi/downloads.html

[GK2]   J. R. GALANTE and V. KALOSHIN, *Destruction of invariant curves in the restricted
         circular planar three body problem using the ordering condition*, preprint,
         available at http://www-users.math.umd.edu/˜joepi/downloads.html

[GPS]   H. GOLDSTEIN, C. P. POOLE, and J. L. SAFKO, *Classical Mechanics*, 3rd ed. Addison
         Wesley, 2001.

[IEEE]   IEEE, *Standard for Binary Floating-Point Arithmetic* (ANSI-IEEE Std 754-1985).

[J]   I. JUNGREIS, *A method for proving that monotone twist maps have no invariant circles*,
         Ergodic Theory Dynam. Systems **11** (1991), 79–84. MR 1101085

[K]   V. KALOSHIN, *Geometric proofs of Mather's connecting and accelerating theorems*,
         Topics in Dynamics and Ergodic Theory, London Math. Soc. Lecture Note Ser.
         310, Cambridge Univ. Press, Cambridge, 2003, 81–106. MR 2052276

[KM]   U. W. KULISCH and W. L. MIRANKER, "Computer arithmetic in theory and practice" in *Computer Science and Applied Mathematics*, Academic Press, New York, 1981. MR 0606741

[LS]   J. LLIBRE and C. SIMO, *Oscillatory solutions in the planar restricted three-body problem*, Math. Ann. **248** (1980), 153–184. MR 0573346

[M1]   J. N. MATHER, *Variational construction of connecting orbits*, Ann. Inst. Fourier (Grenoble) **43** (1993), 1349–1386. MR 1275203

[M2]   ———, *Variational construction of orbits of twist diffeomorphisms,* J. Amer. Math. Soc. **4** (1991), 207–263. MR 1080112

[MF]   J. N. MATHER and G. FORNI, " Action minimizing orbits in Hamiltonian systems" in *Transition to Chaos in Classical and Quantum Mechanics (Montecatini Terme, 1991)*, Lecture Notes in Math. **1589**, Springer, Berlin, 1994, 92–186. MR 1323222

[MS]   D. MCDUFF and D. SALAMON, *Introduction to Symplectic Topology*, 2nd ed. Oxford Math. Monogr., Clarendon Press, Oxford Univ. Press, New York, 1998. MR 1698616

[McG]   R. MCGEHEE, *A stable manifold theorem for degenerate fixed points with applications to celestial mechanics,* J. Differential Equations **14** (1973), 70–88. MR 0362403

[Mo1]   J. MOSER, *Recent developments in the theory of Hamiltonian systems*, SIAM Rev. **28**, (1986), 459–485. MR 08067679

[Mo2]   ———, *Monotone twist mappings and the calculus of variation*, Ergodic Theory Dynam. Systems **6** (1986), 401–413. MR 0863203

[Mo3]   ———, *Stable and Random Motions in Dynamical Systems*: *With special emphasis on celestial mechanics*, Princeton Landmarks in Math., Princeton Univ. Press, Princeton, 2001. MR 1829194

[MZ]   M. MROZEK and P. ZGLICZYŃSKI, *Set arithmetic and the enclosing problem in dynamics*, Ann. Polon. Math. **74** (2000), 237–259. MR 1808998

[NASA]   Available at: http://nssdc.gsfc.nasa.gov/planetary/factsheet/sunfact.html and http://nssdc.gsfc.nasa.gov/planetary/factsheet/jupiterfact.html

[PB]   T. Y. PETROSKY and R. BROUCKE, *Area-preserving mappings and deterministic chaos for nearly parabolic motions*, Celestial Mech. **42** (1987/88), 53–79. MR 0966482

[R]   E. D. RAINVILLE, *Elementary Differential Equations*, 2nd ed. Macmillan, New York, 1958. MR 0089956

[S]   K. F. SIBURG, *The Principle of Least Action in Geometry and Dynamics*, Lecture Notes in Math. **1844**, Springer, Berlin, 2004. MR 2076302

[Si]   K. SITNIKOV, *The existence of oscillatory motions in the three-body problem*, Dokl. Akad. Nauk SSSR **133** (1960), 303–306; English translation in Sov. Phys., Dokl. **5** (1960), 647–650. MR 0127389

[SM]   C. L. SIEGEL and J. K. MOSER, *Lectures on Celestial Mechanics*, trans. C. I. Kalme, Grundlehren Math. Wiss. **187**, Springer, New York, 1971. MR 0502448

[WZ]   D. WILCZAK and P. ZGLICZYŃSKI, *The C^r Lohner-algorithm*, preprint, arXiv:0704.0720v1 [math.NA]

[X1]   Z. XIA, *Arnold diffusion and instabilities in hamiltonian dynamics*, preprint.

[X2]   ———, *Melnikov method and transversal homoclinic points in the restricted three-body problem*, J. Differential Equations **96** (1992), 170 – 184. MR 1153314

[Z]   P. ZGLICZYNSKI, C^1 *Lohner algorithm*, Found. Comput. Math. **2** (2002), 429 – 465. MR 1930946

Galante
Laurel, Maryland 20723, USA; joepi@math.umd.edu

Kaloshin
Department of Mathematics, University of Maryland, College Park, Maryland 20742 – 4015, USA; kaloshin@math.umd.edu